IOWA STATE UNIVERSITY
Digital Repository

Retrospective Theses and Dissertations

Iowa State University Capstones, Theses and Dissertations

1988

Generation, properties, and order packing of monodispersed spherical colloid particles of yttrium hydroxy-carbonate: A colloidal route to minimizing voids in ceramics

Paul Mwesigwa-Kayima
Iowa State University

Follow this and additional works at: https://lib.dr.iastate.edu/rtd

 Part of the Physical Chemistry Commons

Recommended Citation
Mwesigwa-Kayima, Paul, "Generation, properties, and order packing of monodispersed spherical colloid particles of yttrium hydroxy-carbonate: A colloidal route to minimizing voids in ceramics " (1988). *Retrospective Theses and Dissertations*. 9702.
https://lib.dr.iastate.edu/rtd/9702

This Dissertation is brought to you for free and open access by the Iowa State University Capstones, Theses and Dissertations at Iowa State University Digital Repository. It has been accepted for inclusion in Retrospective Theses and Dissertations by an authorized administrator of Iowa State University Digital Repository. For more information, please contact digirep@iastate.edu.

www.manaraa.com

INFORMATION TO USERS

The most advanced technology has been used to photograph and reproduce this manuscript from the microfilm master. UMI films the original text directly from the copy submitted. Thus, some dissertation copies are in typewriter face, while others may be from a computer printer.

In the unlikely event that the author did not send UMI a complete manuscript and there are missing pages, these will be noted. Also, if unauthorized copyrighted material had to be removed, a note will indicate the deletion.

Oversize materials (e.g., maps, drawings, charts) are reproduced by sectioning the original, beginning at the upper left-hand corner and continuing from left to right in equal sections with small overlaps. Each oversize page is available as one exposure on a standard 35 mm slide or as a 17″ × 23″ black and white photographic print for an additional charge.

Photographs included in the original manuscript have been reproduced xerographically in this copy. 35 mm slides or 6″ × 9″ black and white photographic prints are available for any photographs or illustrations appearing in this copy for an additional charge. Contact UMI directly to order.

Accessing the World's Information since 1938

300 North Zeeb Road, Ann Arbor, MI 48106-1346 USA

Order Number 8825423

Generation, properties, and order packing of monodispersed spherical colloid particles of yttrium hydroxy-carbonate: A colloidal route to minimizing voids in ceramics

Mwesigwa-Kayima, Paul, Ph.D.

Iowa State University, 1988

U·M·I
300 N. Zeeb Rd.
Ann Arbor, MI 48106

PLEASE NOTE:

In all cases this material has been filmed in the best possible way from the available copy. Problems encountered with this document have been identified here with a check mark __✓__.

1. Glossy photographs or pages __✓__
2. Colored illustrations, paper or print _____
3. Photographs with dark background __✓__
4. Illustrations are poor copy _____
5. Pages with black marks, not original copy __✓__
6. Print shows through as there is text on both sides of page _____
7. Indistinct, broken or small print on several pages _____
8. Print exceeds margin requirements _____
9. Tightly bound copy with print lost in spine _____
10. Computer printout pages with indistinct print _____
11. Page(s) _____ lacking when material received, and not available from school or author.
12. Page(s) _____ seem to be missing in numbering only as text follows.
13. Two pages numbered _____. Text follows.
14. Curling and wrinkled pages _____
15. Dissertation contains pages with print at a slant, filmed as received _____
16. Other _____

_____

_____

U·M·I

Generation, properties, and order packing of monodispersed spherical colloid particles of yttrium hydroxy-carbonate: A colloidal route to minimizing voids in ceramics

by

Paul Mwesigwa-Kayima

A Dissertation Submitted to the
Graduate Faculty in Partial Fulfillment of the
Requirements for the Degree of
DOCTOR OF PHILOSOPHY

Department: Chemistry
Major: Physical Chemistry

Approved:

Signature was redacted for privacy.

In Charge of Major Work

Signature was redacted for privacy.

For the Major Department

Signature was redacted for privacy.

For the Graduate College

Iowa State University
Ames, Iowa

1988

TABLE OF CONTENTS

LIST OF FIGURES

LIST OF TABLES

I. INTRODUCTION

A. General Introduction

High-technology ceramics are subjects of growing research and development attention. They have excellent mechanical properties under heavy stress, outstanding electrical and optical properties, and exceptional resistance to high temperature and corrosive environments. They are also usually lighter than metals.

This wide range of properties, coupled with the fact that ceramics are generally made from low-cost and abundant raw materials, is the basis of usefulness of ceramics, making them possible substitutes for alloy materials for use in energy applications in high technology systems. In fact, the stability of ceramic materials to high temperatures makes them more efficient above metallurgical temperature limits.

Because these ceramics have high heat resistance, they are used in automotive engines, burner nozzles, and heat exchangers. Their special electrical properties are useful in capacitors, piezoelectric devices, thermistors, solar cells, and integrated-circuit substrates. Their optical properties make them of value as infrared transmission windows, as well as in lasers and high-pressure sodium vapor lamps. Because of their hardness and wear resistance, they find use in cutting tools and bearings. And because some

are biocompatible, they are used as substitutes for bones and joints and in artificial heart valves. Their light weight properties are important in aircraft, missile, and spacecraft applications.

Despite their many virtues, most ceramics have had their applications as high performance materials greatly limited because of their most glaring defect - brittleness, leading to severe failure. Besides, the properties of ceramics are more sensitive to imperfections than those of metals. Pores at grain boundaries or impurity inclusions, for example, may be acceptable in a metal but disastrous in a ceramic.

Another significant shortcoming is the difficulty to make advanced ceramic parts with uniform physical properties from one batch to the next or even within a single batch. As a result, ceramic parts often fail to meet expected performance. To a large extent, this is attributed to the fact that the basic science behind the various processing stages in the fabrication of ceramics is not well understood, and therefore structures with desired and controlled microstructures cannot be prepared. Hence, "the major and overriding problem of high performance ceramics is that components with desired properties and microstructures cannot be reliably and reproducibly manufactured" (1). In the past, ceramic formulation and fabrication has been more of an art than a science. Now, however, the processing of ceramics must of necessity be based on scientific knowledge and theory.

The conventional and traditional way to make a fine powder is to grind a bulk material and pass it through a fine sieve. A problem with this approach is that, although the powder may be relatively fine, its particles are not uniform in size and shape. This results in a final sintered product of high and uncontrolled porosity, with voids many times larger than the size of the particles. These voids, by acting as stress concentrators, ultimately may cause a part to fail, making it unreliable. Besides, the properties of such a product are difficult to reproduce. Furthermore, the very act of grinding the material may introduce metallic or ceramic impurities.

In recent years, one of the biggest thrusts in ceramics research has been to develop materials with greatly improved mechanical reliability, usually by improving their fracture toughness. One approach has been to reduce the size and concentration of pre-existing flaws in ceramics - for example, through the use of pure, uniform, submicron spherical particles. Such particles could be densely packed in an orderly manner. When sintered, they produce a ceramic with very little void space and a minimum of tiny cracks that may form much larger cracks when the ceramic is later subjected to stress.

The considerable amount of work done and the success attained in preparing particles of uniform size and shape cannot be disputed. This provides a breakthrough in the

ability to control the microstructure of ceramic materials. However, a lot of research still needs to be invested in packing these uniform powders in order to achieve highly dense products of high reliability and reproducibility. Although it is known that uniform spherical particles can be orderly packed in a close-packed arrangement of high coordination number, this fact has apparently not been maximally exploited in the fabrication of highly dense ceramics. It is this problem that the work presented in this dissertation attempts to address using principles of colloid science.

B. Objective

The purpose of this study, therefore, is to prepare and characterize highly monodispersed spherical colloid particles of yttrium (hydrous) oxide (2), a precursor material for making yttria (Y_2O_3). These sols will be prepared by kinetically controlling the decomposition of urea at elevated temperatures in aqueous solutions in the presence of ytrrium ions. Efforts will also be aimed at establishing the mechanisms of nucleation and growth leading to these monodisperse sols. Routes leading to formation of ordered lattices of these particles will be sought. The processes to be investigated are reversible flocculation in the secondary minimum of the particle interaction potential energy function and ordering of the Kirkwood - Alder

character. The basic idea behind the former process is to achieve an ordered colloid in the secondary minimum, then to "freeze" this ordered structure by forcing it to coagulate irreversibly in the primary minimum. It is hoped that these processes can be used to develop ordering optimally conducive to production of ceramics approaching theoretical density.

Yttria is important as a refractory material due to its high melting point, low chemical activity, and good thermal shock resistance. It is used both as a matrix and dopant in electronic, optical, magnetic, and nuclear technologies.

II. LITERATURE REVIEW

A. Preparation of Uniform Colloid Particles

The quest of colloid scientists for ways of preparing particles of uniform size and shape is as old as colloid science itself. Originally, scientists were motivated by curiosity, but soon monodispersed systems were to serve as useful models in checking theories of fundamental aspects of colloid science. Now the importance of uniform powders in many areas of modern technology like ceramics, catalysis, pigments, films, and coatings is becoming increasingly more obvious. In fact, nature has shown that uniform colloid particles can form if the conditions are right. The beautiful iridescence of opals, for example, is due to their structure, which is an aggregate of regular microspheres of silica (3). Iler (4) was the first to reproduce the conditions necessary for the formation of an opal-like material by a one-year-long sedimentation of monodisperse silica particles.

Numerous monodispersed colloids have been reported in literature. But probably the most systematic and comprehensive program which has resulted in a large variety of exceedingly uniform inorganic and organic colloids is that due to Matijevic et al. and beautifully reviewed elsewhere (5). The techniques employed can be classified into three categories: (a) precipitation from homogeneous

solutions by (i) forced hydrolysis, (ii) controlled release of anions, and (iii) controlled release of cations; (b) phase transformation; and (c) reaction with aerosols. Several types of monodisperse powders (e.g., TiO_2 (6, 7), SiO_2 (8), $BaTiO_3$ (9), ZnO (9), ZrO_2 (9)) have also been generated by controlled hydrolysis of metal alkoxides in alcohol solutions.

B. High Density Ceramics

A new field of research in inorganic colloids known as the sol-gel process emerged during the early 1960s. Sol-gel processing techniques are often divided into two general methods. In one case, colloidal dispersions (i.e., sols) of fine particles are prepared and subsequently destabilized, or gelled, by chemical and/or thermal treatments. In another method, organometallic compounds are hydrolyzed and polymerized. Gelation occurs as growing polymeric species agglomerate and crosslink to form an extensive, three-dimensional network. First applied to the fabrication of highly dense oxide fuels for nuclear reactors (10-13), the techniques are now being used increasingly to produce a range of materials for non-nuclear applications in fields such as coatings, fibers, abrasives, catalysts, ceramics, glasses, ceramic-glasses, and composites. The following references (14-25) cited and the references therein are but a few of the many references documented in literature on this subject.

Fine particles produced by flame oxidation of metal halides or organometallic compounds in a gas/oxygen flame have also been used to produce bodies that sinter to high densities at relatively low temperatures (26). Recently, ceramic powder compacts that sinter to near theoretical densities have been prepared by packing monosized spherical particles in an ordered way by gravitational or centrifugal settling (6, 27-29).

C. Ordering of Colloidal Dispersions

Monodisperse polymer latices have long been known to form ordered or disordered structures depending on conditions (30-35). The ordered structures give bright iridescence if the center-to-center distance between the particles is comparable with the wavelength of visible light, while the disordered structures generally look milky white. Iridescence has been correctly attributed to Bragg reflection of visible light from ordered arrays of particles by Luck et al. (32). They have also suggested the secondary minimum of the particle interaction potential energy function as the cause of formation of ordered structures. The detailed structure of the distribution of particles has been determined by a light scattering technique (36-39). Direct observation of a regular hexagonal or cubic distribution of the latex particles has been successfully carried out by Kose et al. (40) using a metallurgical microscope as an ultramicroscope.

Determination of interparticle distances has revealed that ordered structures form even at large interparticle spacings (41). This has led some workers to conclude that the electric repulsion between particles is the cause of order formation since the van der Waals forces to which the secondary minimum is due cannot be effective at such large distances. This seems to be supported by Hiltner and Krieger's (42) observation that the ordered structure extended over the whole body of the latices under the experimental conditions they worked with.

Hachisu et al. (43) have studied the conditions for the occurrence of ordered and disordered structures, and they have constructed a phase diagram of polystyrene latex particles in KCl solution with the solid content in volume fraction as the ordinate and the logarithm of the electrolyte concentration as the abscissa (Figure 1). On the basis of these experimental results, the van der Waals force and hence the secondary minimum has been rejected as the cause of phase separation for two reasons. Firstly, the van der Waals force is shown to be ineffective even at as high volume fraction as 0.35. Secondly, the secondary minimum is deep at high electrolyte concentrations and becomes shallow at low electrolyte concentrations. Therefore, if order formation had been caused by flocculation in the secondary minimum, dissolution of the ordered structure would have taken place when the

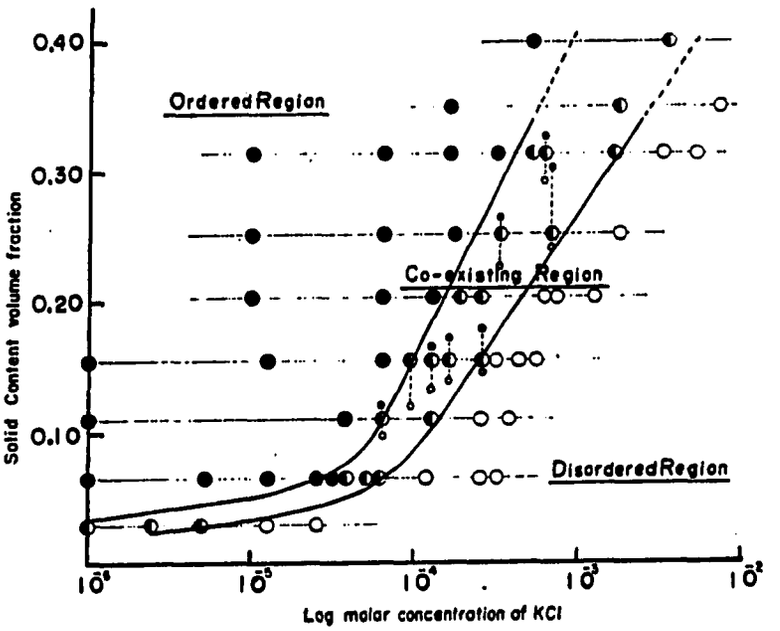

Figure 1. Phase diagram of polystyrene latex with a particle diameter of 1700 Å containing KCl in its aqueous phase; ●, ordered state; O, disordered state; ◐, state of coexistence; •, volume fraction of the sediment; o, volume fraction of the supernatant; • and o linked to a ◐-mark by dotted lines refer to the separated two phases in the state represented by ◐, respectively. (from reference 43)

electrolyte concentration was reduced while maintaining the solid content constant. Since electric repulsion also cannot yield phase separation, these workers have concluded that the present theory of colloidal interaction, in its present form, is not able to account for this phenomenon.

However, this is a fact that was not recognized by Barnes et al. (44), who attempted to explain Hachisu's results on the basis of pure electric repulsive forces between particles. In their analysis, spherical colloidal particles are treated as "effective spheres" whose sizes are determined by the thickness of the double layer. This is combined with a generalization of Kirkwood and Alder's suggestion (45, 46) that in purely repulsive systems, there exists a critical particle number density above which only crystalline structures with long-range order are possible. Therefore, as the electrolyte concentration is reduced, the radius and hence the volume fraction of effective spheres increases, since the spheres are confined to a fixed volume by the dispersion medium. At some point, the interaction among the randomly arranged effective spheres is such that it becomes more favorable energetically to accommodate some of these spheres in an ordered lattice. As the electrolyte concentration is further reduced, the effective spheres can only be accommodated without incurring large repulsive energies by a steady increase in the fraction of particles in the close-packed arrangement.

Studying highly charged latex dispersions by the ultramicroscopic method, Ise et al. (47, 48) have found that the interparticle center-to-center distance of the ordered phase is large (of the order of 10^4 Å). This fact strongly suggests that the van der Waals attraction is not significant in the ordering, and that the dominant interaction at such large separations must be coulombic. However, they do not attribute the existence of order to long-range repulsive forces because of the observation that the interparticle separation was smaller than the average value calculated from the latex concentration assuming a uniform simple cubic distribution. This inequality relation suggests the existence of a two-state structure, which consists of ordered regions of higher particle number density and less dense disordered regions. Such a two-state structure is the most direct evidence of interparticle attraction. If attractive interaction does not exist, or if only repulsive interaction is operating, they argue, a localized ordered array is impossible. Condensed systems with free boundary or surface cannot exist without attractive interaction. In other words, the ordered structure must be space filling if it is formed by repulsion only. From these observations they concluded that there is a coulombic attractive interaction between the latex particles of similar charge through the intermediary of the counterions.

It has been pointed out (47, 48) and theoretically elucidated (49) that this coulombic attraction is balanced by repulsive forces between particles, creating a "secondary minimum" which is much farther from the origin of the potential energy curve than the conventional secondary minimum due to van der Waals forces. In fact, Hachisu's results (40) have been successfully interpreted in light of this "secondary minimum" (49). Although it is not taken into consideration in most of the theories of colloid particles and polyelectrolytes, coulombic attraction has a sound physical basis, as lucidly pointed out by Feynman et al. (50), who stated, "attraction arises because the repulsion of likes and attraction of unlikes will tend to bring unlikes closer together and push likes farther apart. Then the repulsion will be less than the attraction".

D. Decomposition of Urea

The decomposition of urea in aqueous media at elevated temperatures has been extensively studied by several investigators (51-63) under various conditions of concentration, pH, temperature, and ionic strength. In almost every case, investigators have attempted to establish the mechanism of decomposition, besides determining the rate constants and/or the activation energies.

Two mechanisms for the decomposition of urea have been postulated and enthusiastically defended by their authors.

In a series of papers attempting to establish the structure of urea as (I) rather than the conventional carbamide structure (II), Werner (54, 55) presented the scheme:

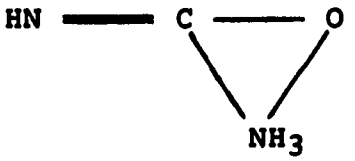

$$\longrightarrow \quad HNCO + NH_3 \qquad [1]$$

(I)

and then presumably:

$$HNCO + NH_3 \rightleftharpoons NH_4^+ + NCO^- \qquad [2]$$

Fawsitt (52, 53) felt that this formulation was unnecessary and assumed instead the following formulation:

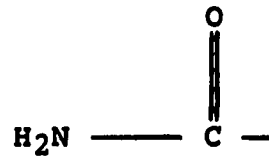

$$\longrightarrow \quad NH_4^+ + CNO^- \qquad [3]$$

(II)

Whatever the structure of urea, it is now generally accepted that urea initially converts to ammonium cyanate in a slow, first-order rate-determining step:

$$CO(NH_2)_2 \longrightarrow NH_3 + HNCO \rightleftharpoons NH_4^+ + NCO^- \qquad [4]$$

followed by a rapid hydrolysis of the cyanate ion to give:

$$NCO^- + 2H^+ + H_2O \longrightarrow NH_4^+ + CO_2 \text{ (in acidic media)} \qquad [5]$$

$$NCO^- + 2H_2O \longrightarrow NH_4^+ + CO_3^{2-} \qquad [6]$$

and/or (in neutral media)

$$NCO^- + 3H_2O \longrightarrow NH_4^+ + 2OH^- + CO_2 \qquad [7]$$

$$NCO^- + OH^- + H_2O \longrightarrow NH_3 + CO_3^{2-} \text{ (in basic media)} \qquad [8]$$

Other solution equilibrium processes of interest are:

$$NH_3 + H_2O \rightleftharpoons NH_4OH \rightleftharpoons NH_4^+ + OH^- \quad [9]$$

$$CO_2 + H_2O \rightleftharpoons H_2CO_3 \rightleftharpoons H^+ + HCO_3^- \rightleftharpoons 2H^+ + CO_3^{2-} \quad [10]$$

First-order rate constants for the decomposition of urea at different experimental conditions, which are relevant to this study, are given in APPENDIX A.

III. EXPERIMENTAL

A. Materials and Instrumentation

The chemicals used in this study were of highest purity grade and they were used without further purification. Except for yttrium nitrate (99.9%), wich was supplied by Johnson Mathey, Inc., all other chemicals were obtained from Fisher Scientific Co. The copper grids used in transmission electron microscopy were obtained from Structure Probe, Inc. Unless otherwise stated, the water used was quadruply distilled in all-glass-ware. All glassware was cleaned by soaking in chromic acid followed by thorough rinsing in singly distilled water.

For all centrifugation purposes, either a Sargent International clinical centrifuge model CL or a Du Pont sorvall RC-5B refrigerated superspeed centrifuge was used. A Buehler Ultramet II sonic bath was used to break up agglomerated particles in dispersions. Shape and size analyses were done by use of a type HU-125 Hitachi transmission electron microscope (TEM) and/or a Cambridge S-200 scanning electron microscope (SEM), while electron diffraction studies were done on a JEOL 100 CX electron microscope. Samples for microscopic examinations in the SEM were sputter coated with gold using a Technics Hummer II sputter coater. Transmission electron micrographs were analysed for size using a Lemont Scientific DA-10 image

analysis system. Electrophoretic measurements were done on a model 500 Laser Zee Meter. Thermal analyses were performed on a Du Pont 1090 thermal analyzer, while X-ray photoelectron spectroscopy (XPS) was done on an AEI 200B spectrometer. A Leco carbon analyzer was used to determine the carbonate content of the powders. For turbidimetric determinations a model 320 Perkin Elmer UV-VIS spectrophotometer was utilized, while pH measurements were done either on a Corning pH meter 130 or an Orion Research model 601A digital ionalyzer.

B. Sol Preparation and Characterization

Numerous preliminary experiments using an array of conditions (yttrium nitrate, urea and nitric acid concentrations, temperature, and duration of reaction) were carried out in order to determine the best conditions for preparing particles uniform in both shape and size. In each experiment, 20 cm^3 of solution containing yttrium nitrate and urea (and in some cases nitric acid) were reacted at a known constant temperature (70 - 100^oC) in a screw-cap-covered test-tube immersed in a thermostatic bath for a known period of time.

The precipitates were washed thoroughly (up to six times) with singly distilled water by centrifugation and decantation. They were redispersed in appropriate solvents by ultrasonication. Shape and size analyses were done by

use of TEM and/or SEM. Average particle sizes and their distributions were obtained from analyses of electron photomicrographs using an image analyzer. In some cases, average sizes were determined manually by measuring the diameters of images in the electron photomicrographs using a ruler, and then using the photomicrograph magnification factor to calculate true diameters. At least 200 particles were sized for each sample, which gives a size distribution with an expected accuracy of 1% (64). Electrophoretic measurements were used to characterize the charge on the surfaces of particles, while the chemical composition of the precipitates was investigated using chemical, thermal, and X-ray photoelectron spectroscopic analyses.

1. Particle size dependence on urea concentration

20 cm^3 solutions, each containing 0.02 M $Y(NO_3)_3$ but different amounts of urea (0.05 - 0.75 M), were reacted at 100°C for 32.5 minutes. After the reaction mixtures had cooled to room temperature, the precipitates were washed three times and their particle sizes analyzed.

2. Particle size dependence on $Y(NO_3)_3$ concentration

20 cm^3 solutions, each containing 0.25 M urea but different amounts of $Y(NO_3)_3$ (0.02 - 0.10 M) were reacted at 100°C for 30.2 minutes. After the reaction mixtures had cooled to room temperature, the precipitates were washed three times and their particle sizes analyzed.

3. Sample preparation for TEM

Samples to be examined under the TEM were dispersed in ethanol and diluted to suitable particle concentrations. A tiny drop of the resulting dispersion was applied to a copper grid pre-coated with a carbon film and allowed to dry in air before examination.

4. Sample preparation for SEM

Samples to be examined under the SEM were dispersed in ethanol and diluted to suitable particle concentrations. A drop of the resulting dispersion was applied to an aluminum piece (15 X 5 X 0.5 mm), left to dry in air, and sputter coated with gold (film thickness ~ 100 Å). The aluminum piece was then glued on a specimen mount and inserted into the specimen chamber of the SEM for examination.

5. Electrophoretic measurements

The sol used was prepared by reacting 100 cm^3 of solution, 0.02 M in $Y(NO_3)_3$ and 0.25 M in urea contained in a screw-cap-covered Erlenmeyer flask at 100°C for 1 hour. The precipitate formed was washed four times and redispersed in a 10^{-4} M NaCl solution. Samples of this dispersion were prepared at different pHs and their zeta (ζ)-potentials measured, recording the temperature at each measurement. All ζ-potentials were corrected to a temperature of 20°C. The pHs of the sols were adjusted with HCl and/or NaOH.

6. Analysis of chemical composition of material

A 450 cm^3 solution containing 0.02 M $Y(NO_3)_3$ and 0.25 M urea was allowed to react at 100°C for 1 hour. The precipitate formed was washed six times and dried at 60°C in an oven. The resulting powder was analyzed by thermal gravimetric analysis (TGA), differential thermal analysis (DTA), X-ray photoelectron spectroscopy (XPS), and chemical analysis. For TGA and DTA experiments, a small amount of powder was heated at a constant rate of 10°C/min. from room temperature (20°C) to 1000°C. In order to resolve the various processes that take place during heating, a second TGA run was done. In this run, the sample was heated at constant rate (10°C/min.) to 185°C. The temperature was held steady for 30 minutes until the weight of the sample levelled off before the temperature was allowed to rise again at the original rate. This pattern was repeated holding the temperature constant at 480°C for 45 minutes and at 720°C for 30 minutes. Such a treatment gave sufficient time for the processes to proceed to completion. In another set-up, the sample was heated while the gases coming off were continually detected by a mass spectrometer. XPS analyses were performed on the powder before and after it had been heated to 1000°C. For chemical analyses, the powder was dissolved in HCl and the pH adjusted to 4.5. Yttrium was then determined by titrating with EDTA using xylenol orange as indicator. The carbonate content was determined using a Leco carbon analyzer.

7. Transmission electron diffraction

To determine whether the precipitation product was crystalline or amorphous, a 20 cm^3 solution, 0.02 M in $Y(NO_3)_3$ and 0.25 M in urea was reacted at 100°C for 5 minutes. The precipitate produced was washed six times, redispersed in water, and its transmission electron diffraction pattern taken. An accelerating voltage of 120 kV (corresponding to an electronic wavelength of 0.0335 Å) was used. The sample to photographic plate distance was 46 cm.

8. Particle density determination

A precipitate prepared as in III.B.6 was redispersed in water after washing. The resulting sol was introduced into a clean, dry and pre-weighed 10 cm^3 volumetric flask being careful not to wet the walls of the flask above the sol level. The flask and its contents were then weighed. The sol was allowed to dry at 60°C in an oven after which the flask and the powder were weighed. This process was repeated until a constant weight was obtained. The volume of the flask was standardized by weighing the flask containing water, since the density of water at the temperature of the room was known. The flask was handled using polyethylene gloves during the determination.

C. Nucleation and Growth Studies

1. Induction period measurements

Three series of 20 cm^3 solutions were prepared in screw-cap-covered test-tubes, each containing urea, yttrium nitrate, and nitric acid. In the first series, each solution contained 0.05 M $Y(NO_3)_3$, 0.078 M HNO_3, but different amounts of urea. In the second series, each solution contained 0.05 M $Y(NO_3)_3$, 0.5 M urea, but different amounts of HNO_3. In the third series, each solution contained 0.5 M urea, 0.078 M HNO_3, but different amounts of $Y(NO_3)_3$. All solutions were reacted at 100°C and the time it took the solutions to turn turbid (hereafter called induction period, τ) was recorded.

2. pH measurements

Solutions containing different ratios of urea to $Y(NO_3)_3$ but with no HNO_3 added were prepared and their pHs measured at room temperature (25°C).

3. Measurement of particle growth rate

A 450 cm^3 solution, 0.02 M in $Y(NO_3)_3$ and 0.25 M in urea was allowed to react in a 500 cm^3 screw-cap-covered Erlenmeyer flask at 100°C. Aliquots of the reaction mixture were withdrawn after the induction period at intervals of 5 or 10 minutes, and immediately added to ice-water to quench the reaction. The end of the induction period was taken as

the beginning of particle growth (i.e., zero growth time). The precipitates formed were washed three times and the average sizes and size distributions of the constituent particles determined by TEM.

4. Silica seeded precipitation

A series of precipitation experiments was performed in the presence of spherical silica particles of narrow size distribution. The silica used was the LUDOX SM colloidal silica, a Du Pont product. The characteristics and the determination of the number of silica particles/cm^3 of this sol are given in APPENDIX B. In each experiment, a 21 cm^3 solution 0.05 M in $Y(NO_3)_3$ and 0.24 M in urea, but differing in the number of silica particles it contained, was heated for 35 minutes at 100°C. The induction period for each experiment was recorded. The resulting precipitates were washed three times and the average particle sizes determined by SEM.

D. Stability of Sols and Order Packing

The sol used in this study was prepared and washed as in III.B.6.

1. Stability studies

Stability studies of the sol as a function of pH were done using a turbidimetric method. Absorbances, A of

dispersions were measured in a 1 cm cell at a wavelength of 560 nm as a function of time at various pHs (in the range 7 through 12.3). Absorbance (where $A = \ln (I_o/I)$, I_o and I being intensities of the incident and transmitted light respectively) was measured although it is the scattered light from a suspension that increases with flocculation. The increase in light scattering results in increased turbidity, T and hence increased absorbance of a suspension since:

$$T = \frac{1}{l} \ln \frac{I_o}{I} \qquad [11]$$

where l is the thickness of a suspension traversed by light. PHs were adjusted using NaOH and/or HCl. The initial slope of the trace, which gives the rate of turbidity increase, was taken as a measure of the rate of flocculation.

2. Order - disorder studies

Five aqueous dispersions (hereafter called D1, D2, D3, D4, and D5), each having a particle volume fraction, ϕ of 0.2, were prepared and their pHs adjusted with NaOH to 8.8, 9.1, 9.5, 10.9, and 10.9 respectively. The solid contents of the suspensions were determined by drying to constant weight suspensions of known volume and weight. The density determined in III.B.8 was used for computation of volume fractions. D1 through D4 were left to stand while D5 was spun in a centrifuge at 3,000 rpm for 30 minutes. The

supernatant liquor was decanted off and the solid cake allowed to dry in air at room temperature. A piece of the dried cake was mounted and glued on a sample holder, coated with gold and examined in a SEM.

After two weeks, the pH of D4 was decreased to about 7.4 by slowly and carefully adding 0.15 M HCl acid dropwise without disturbing the system. HCl was allowed to permeate the whole system by diffusion. The system was then spun down in a centrifuge at 3,000 rpm for 30 minutes, before the supernatant liquor was decanted off. After air-drying the resulting cake at room temperature, it was examined in a SEM in the same way as D5.

IV. RESULTS AND DISCUSSION

A. Sol Preparation and Characterization

The incidence of precipitation was preceded by an induction period, τ within which a solution remained clear. The end of the induction period was marked by an abrupt change in the turbidity of the mixture. The turbidity increased continuously with reaction before the white precipitate eventually coagulated and settled. Continued precipitation beyond this point resulted in neck-formation between particles (Figure 2). In all cases investigated, spherical particles were obtained. The widths of the particle size distributions and the average sizes varied with experimental conditions.

With increasing concentrations of urea (in the range 0.05 - 0.75 M), at constant $Y(NO_3)_3$ concentration (0.02 M), temperature (100°C), and length of reaction (32.5 min.), the induction period shortened, the precipitates coagulated and settled earlier, the average sizes of the particles increased, while the widths of the size distributions became increasingly narrower (Table 1). Figure 3 shows transmission electron micrographs of particles obtained at different concentrations of urea.

Increasing the concentration of $Y(NO_3)_3$ (in the range 0.02 - 0.10 M) while maintaining the urea concentration (0.25 M), temperature (100°C), and length of reaction

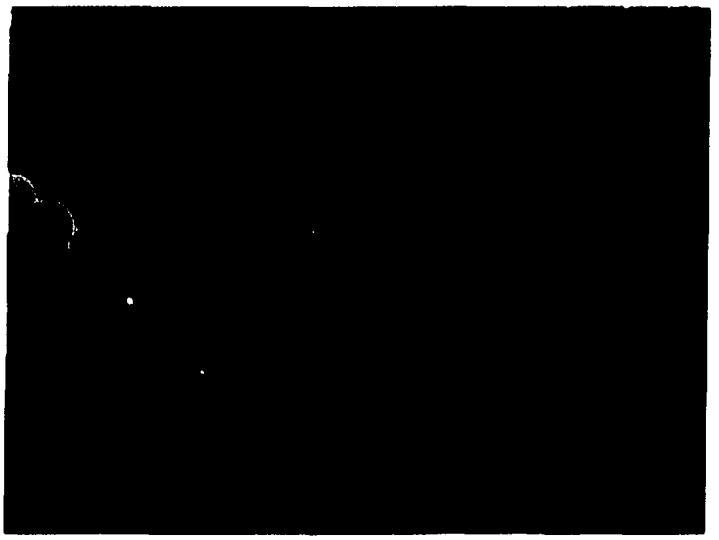

Figure 2. SEM showing neck-formation between particles obtained by heating a solution containing 0.05 M $Y(NO_3)_3$ and 1.0 M urea at 100°C for 33.3 minutes. The precipitate coagulated and settled after 24.9 minutes

Table 1. Variation of average particle diameter and percentage standard deviation with variation in urea concentration. $[Y(NO_3)_3]$=0.02 M; temperature=100°C; length of reaction=32.5 minutes

[Urea]/M	Average Particle Diameter/μ	% Standard Deviation
0.05	0.308	14.7
0.15	0.349	13.3
0.25	0.385	11.1
0.50	0.412	9.30
0.75	0.393	9.18

(b)

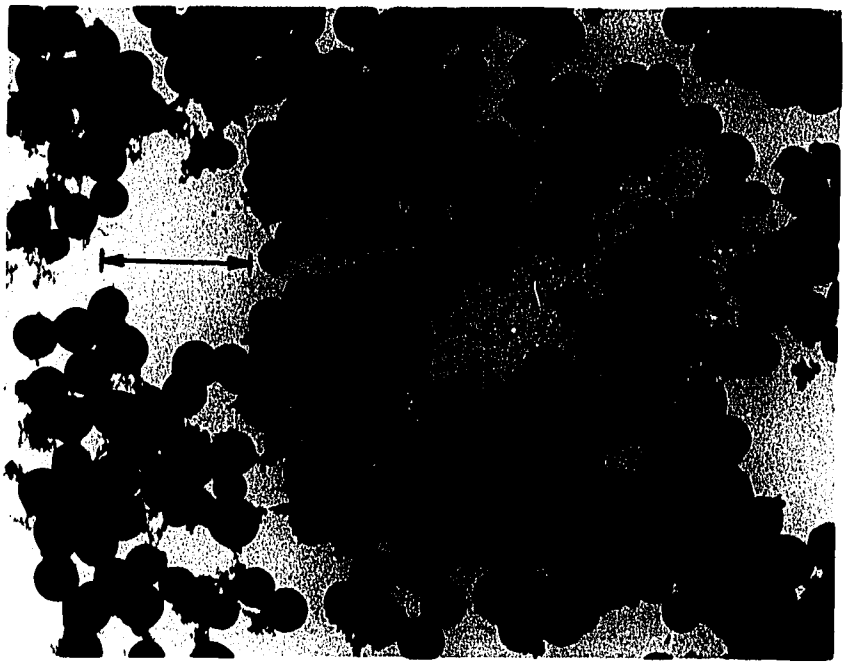

(a)

Figure 3. TEMs of particles obtained by reacting solutions containing 0.02 M $Y(NO_3)_3$ and different concentrations of urea (a) 0.05 M and (b) 0.15 M for 32.5 minutes at 100°C. (bar=1μ)

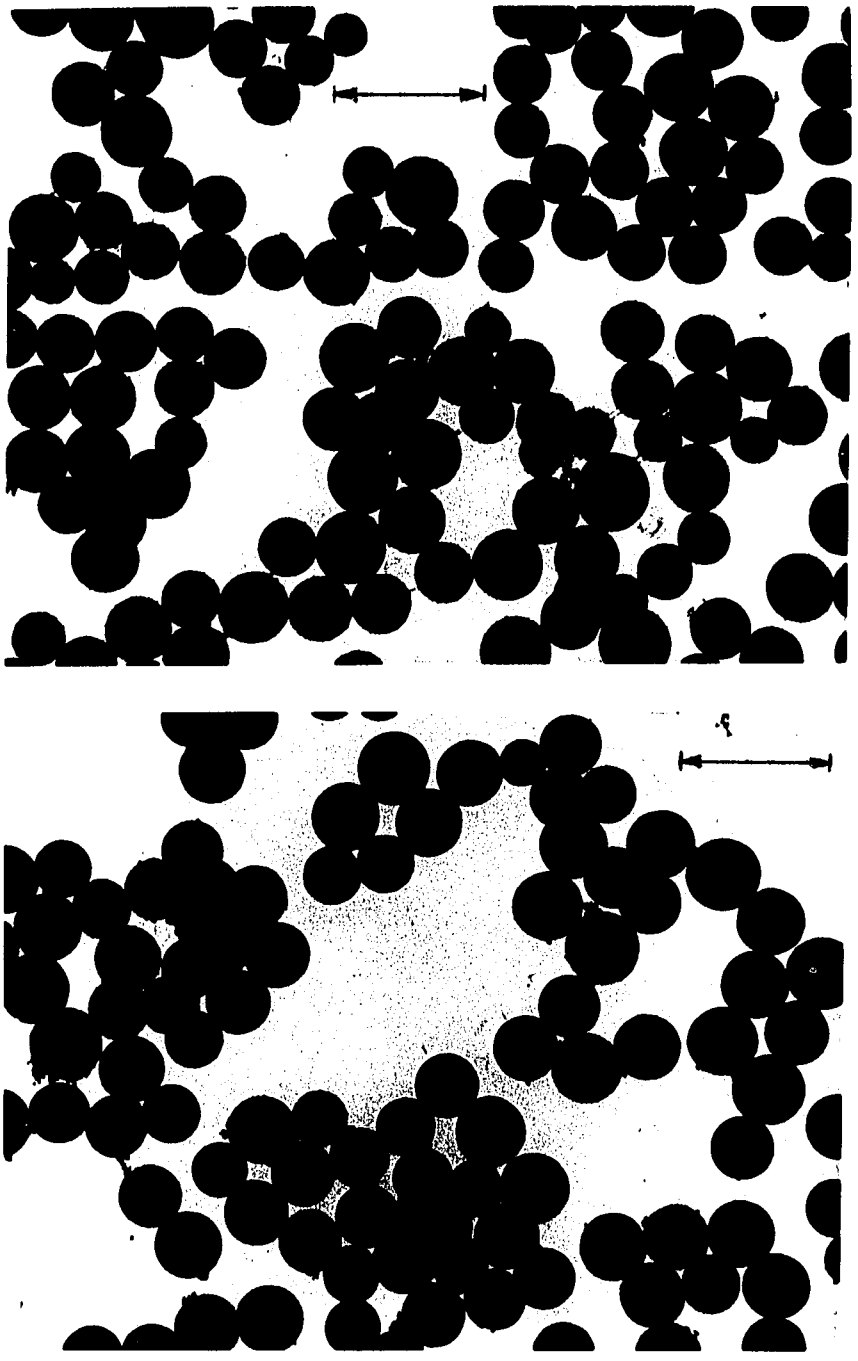

Figure 3. (continued)
(c) 0.25 M and (d) 0.50 M

(e)

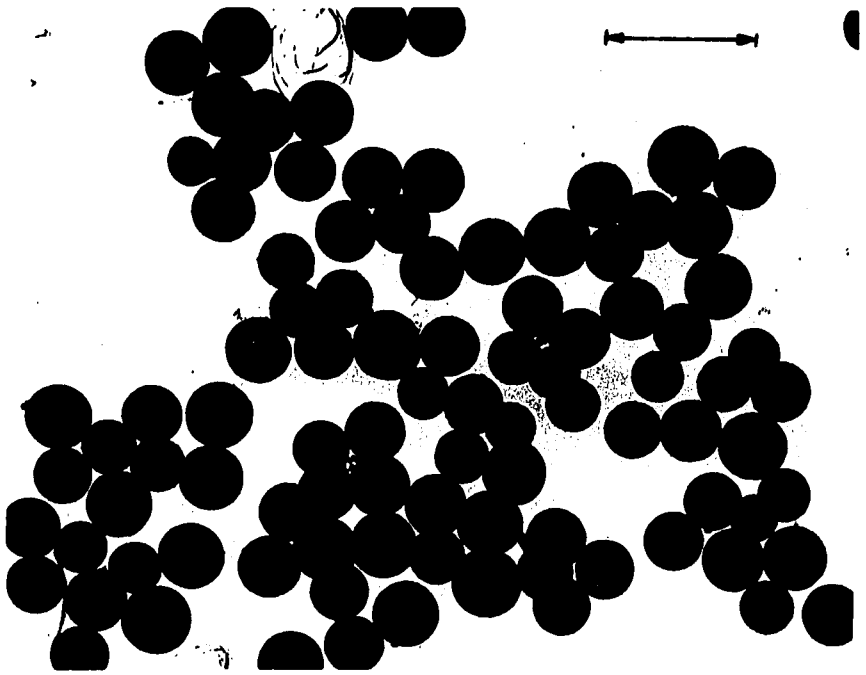

Figure 3. (continued)
(e) 0.75 M

(30.2 min.) constant, lengthened the induction period, resulted in earlier coagulation and settling of precipitates, and produced increasingly smaller particles with broader size distributions (Table 2).

Table 2. Variation of average particle diameter and percentage standard deviation with variation in $Y(NO_3)_3$ concentration. [urea]=0.25 M; temperature=100°C; length of reaction=30.2 minutes

$[Y(NO_3)_3]$	Average Particle Diameter/μ	% Standard Deviation
0.02	0.273	13.9
0.04	0.219	16.4
0.05	0.211	14.7
0.07	-[a]	-[a]
0.10	-[a]	-[a]

[a]Could not be determined due to immense particle coagulation.

Transmission electron micrographs showed an increase in the intensity of agglomeration of particles with increasing $Y(NO_3)_3$ concentration (Figure 4). In fact, particle agglomeration at high $Y(NO_3)_3$ concentration (above 0.05 M) made particle size determinations impossible.

Since the decomposition of urea is capable of producing both hydroxide and/or (bi)carbonate ions, a number of possible yttrium compounds could be formed if the reaction is carried out in the presence of yttrium ions. The nature

(a)

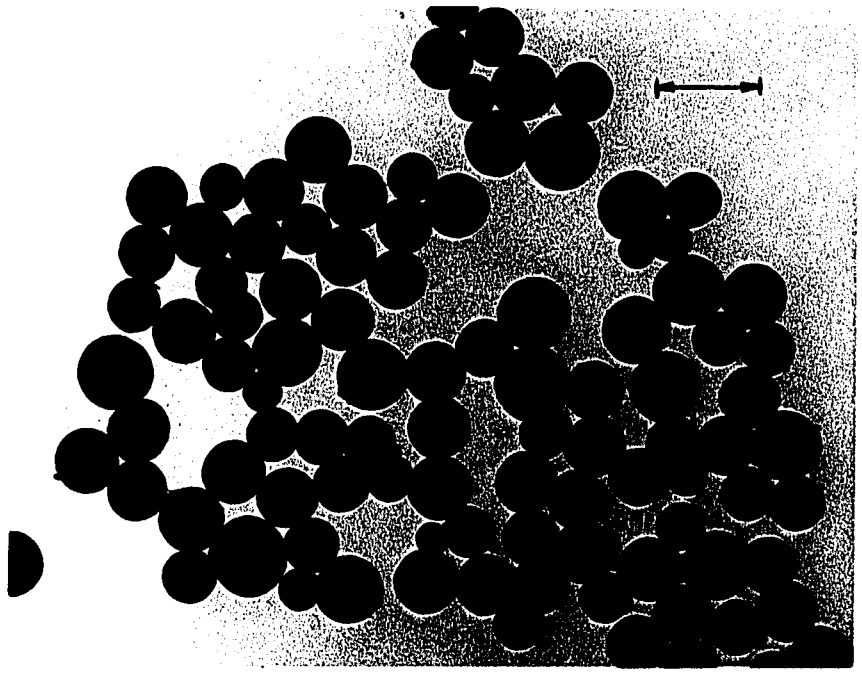

(b)

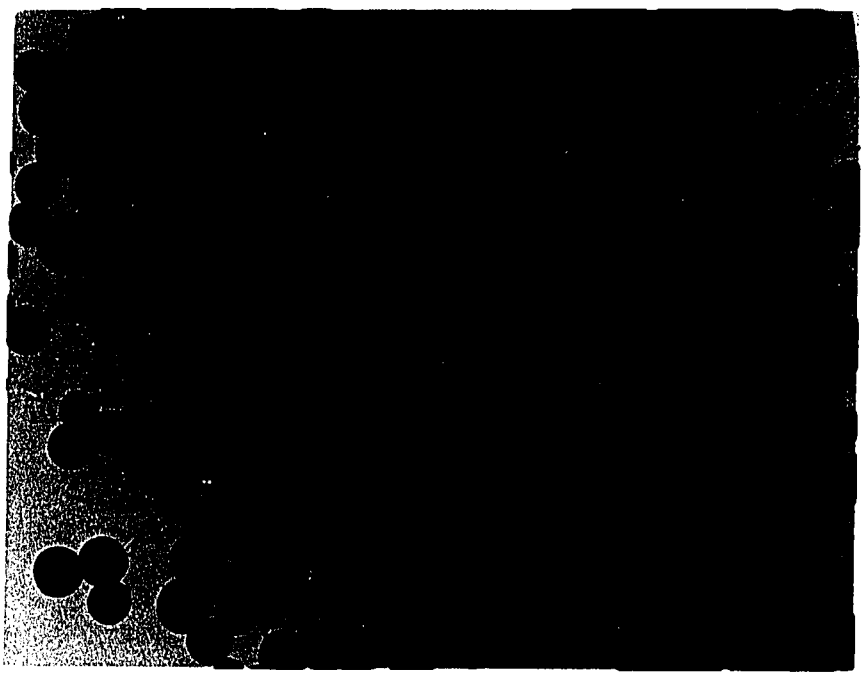

Figure 4. TEMs of particles obtained by reacting solutions containing 0.25 M urea and different concentrations of $Y(NO_3)_3$ (a) 0.02 M and (b) 0.04 M for 30.2 minutes at 100°C. (bar=0.5μ)

(c)

(d)

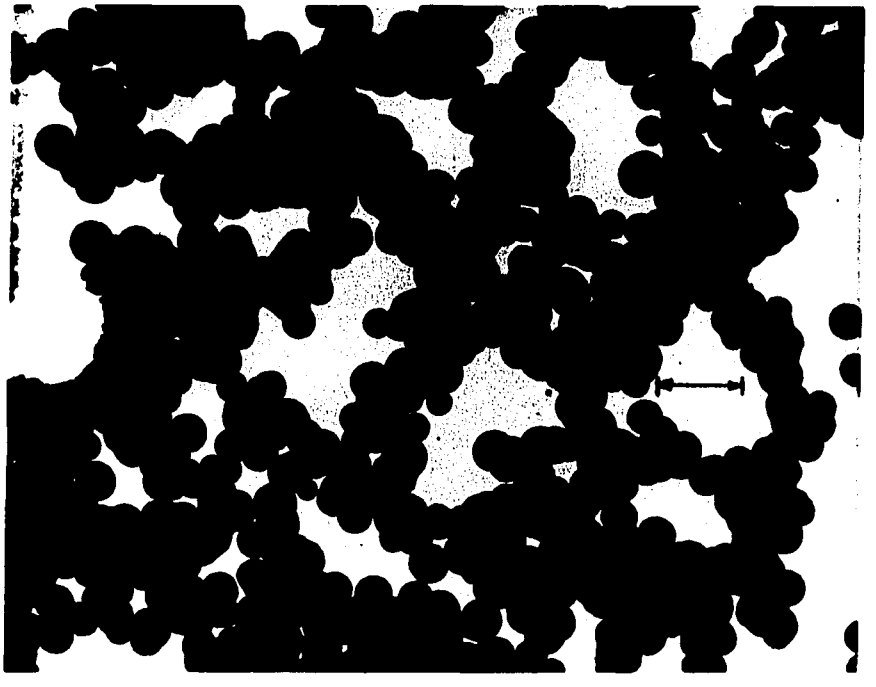

Figure 4. (continued)
(c) 0.05 M and (d) 0.07 M
(bar=0.5μ for c and 0.25μ for d)

(e)

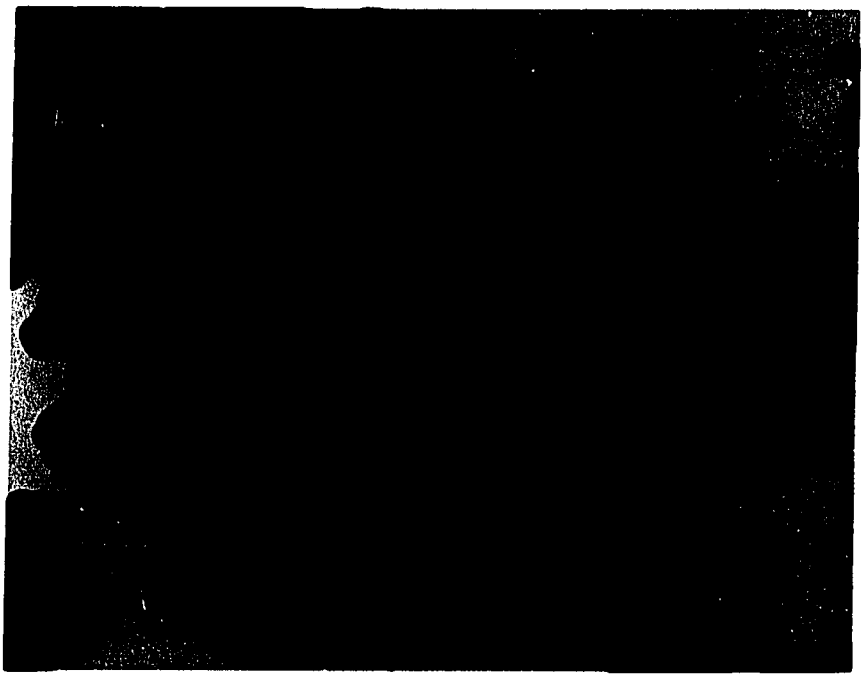

Figure 4. (continued)
(e) 0.10 M
(bar=0.25μ)

of ionic species (and hence yttrium compound) and the rate at which they are generated in solution depend on the concentration of the reactants, and the acidity and temperature of the solution.

It is not surprising, therefore, that by manipulating these experimental parameters, it was possible to generate the precipitating material at a rate that afforded the production of uniform particles. The basic requirement is for all nuclei to be produced in a single burst with additional material being supplied so slowly, that it can find its way to the nuclei without the supersaturation reaching a level at which further nucleation could occur.

Because urea decomposes by a first-order rate law, increasing the urea concentration increases the rate at which the decomposition products (and hence the precipitating species) are generated in solution. Therefore, the nuclei form and begin to grow increasingly earlier. This tends to shorten the induction period and to produce larger particles due to increased growth periods. The assumption that is being made here is that nearly the same number of nuclei is produced in each case. The narrowing of the particle size distributions with increasing urea concentration suggests that the particles grow by a diffusion process. This is discussed in more detail later.

On the contrary, increasing $Y(NO_3)_3$ concentration seems to have a retarding effect on the precipitation reaction.

The nucleation and growth events are delayed, resulting in increased induction periods, reduced growth periods, and diminishing particle sizes. The increasing breadth of the particle size distributions also points to a diffusion controlled growth process.

Measurements of ζ-potentials of particles revealed that at low pH, the particles have a net positive charge, while at high pH they have a net negative charge with an isoelectric point (IEP) of about 7.4 (Figure 5). These results show that the H^+ and OH^- are the potential determining ions. This is a behavior that is shared by most metal (hydrous) oxides (2). In fact, coagulation of the particles during precipitation could partly be explained as a consequence of charge modification on the particle surface due to changes in pH. The pH of a solution (measured at room temperature), that was reacted at 100°C until the onset of turbidity and then rapidly cooled in ice water to arrest the reaction was 6.1. This means that, at the onset of precipitation, the particles are positively charged since the pH is less than 7.4 (the IEP). As the precipitation reaction proceeds, the pH of the dispersion increases while the net positive charge on the particles is reduced. At a pH in the vicinity of the IEP, the net charge becomes too low to maintain a stable sol, resulting in coagulation and subsequent settling. Although the actual pH of the solution would be different at 100°C, it is probable that the IEP would also be different at that temperature.

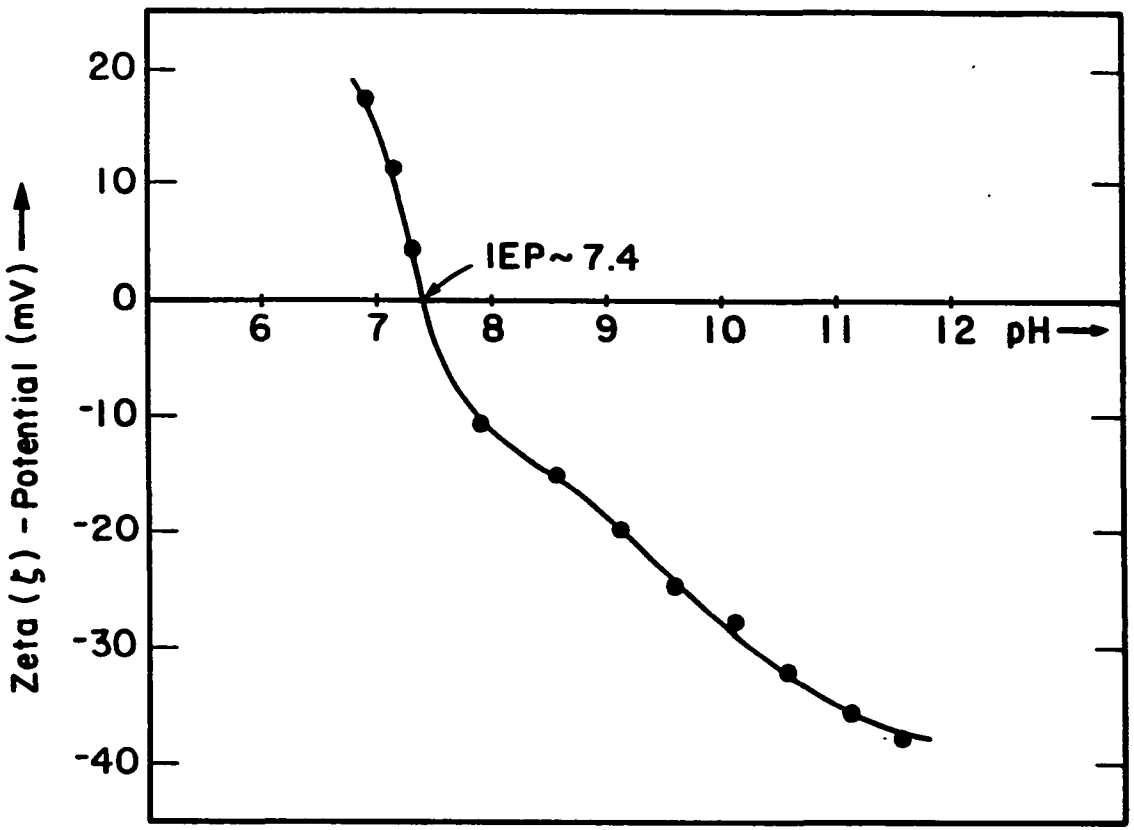

Figure 5. Zeta (ζ)-potentials as a function of pH in a 10^{-4} M NaCl solution for particles obtained by reacting a solution containing 0.02 M $Y(NO_3)_3$ and 0.25 M urea for 1 hr. at 100°C

Another factor that seemed to play a major role in the coagulation of particles is the ionic strength of the dispersion medium. This was evident in preparations involving high concentrations (above 0.05 M) of $Y(NO_3)_3$. These high electrolyte conditions tend to compress the double layers and hence lower the energy barrier between the particles, causing the precipitates to coagulate.

The sedimentation velocity V, of spheres of radius r, density d, in a solvent of viscosity η, density d_s, under gravity g, is given by the classical sedimentation velocity equation:

$$V = \frac{2r^2(d - d_s)g}{9\eta} \qquad [12]$$

The density of the particles was found to be $2.17 g/cm^3$ For particles of radius less than 0.2μ, the maximum sedimentation velocity in water at 100^oC would be 1.3 mm/hr, which could be readily compensated for by random convection currents. Therefore, the instability of the precipitates during preparation cannot be attributed to individual particle sedimentation.

From the TGA (Figure 6) and DTA (Figure 7) curves, it is apparent that three processes take place as the powder is heated at a constant rate of 10^oC/min. from room temperature (20^oC) to 1000^oC. These processes were well resolved in the run that consisted of both dynamic and static temperature conditions (Figure 8). Over the entire range of

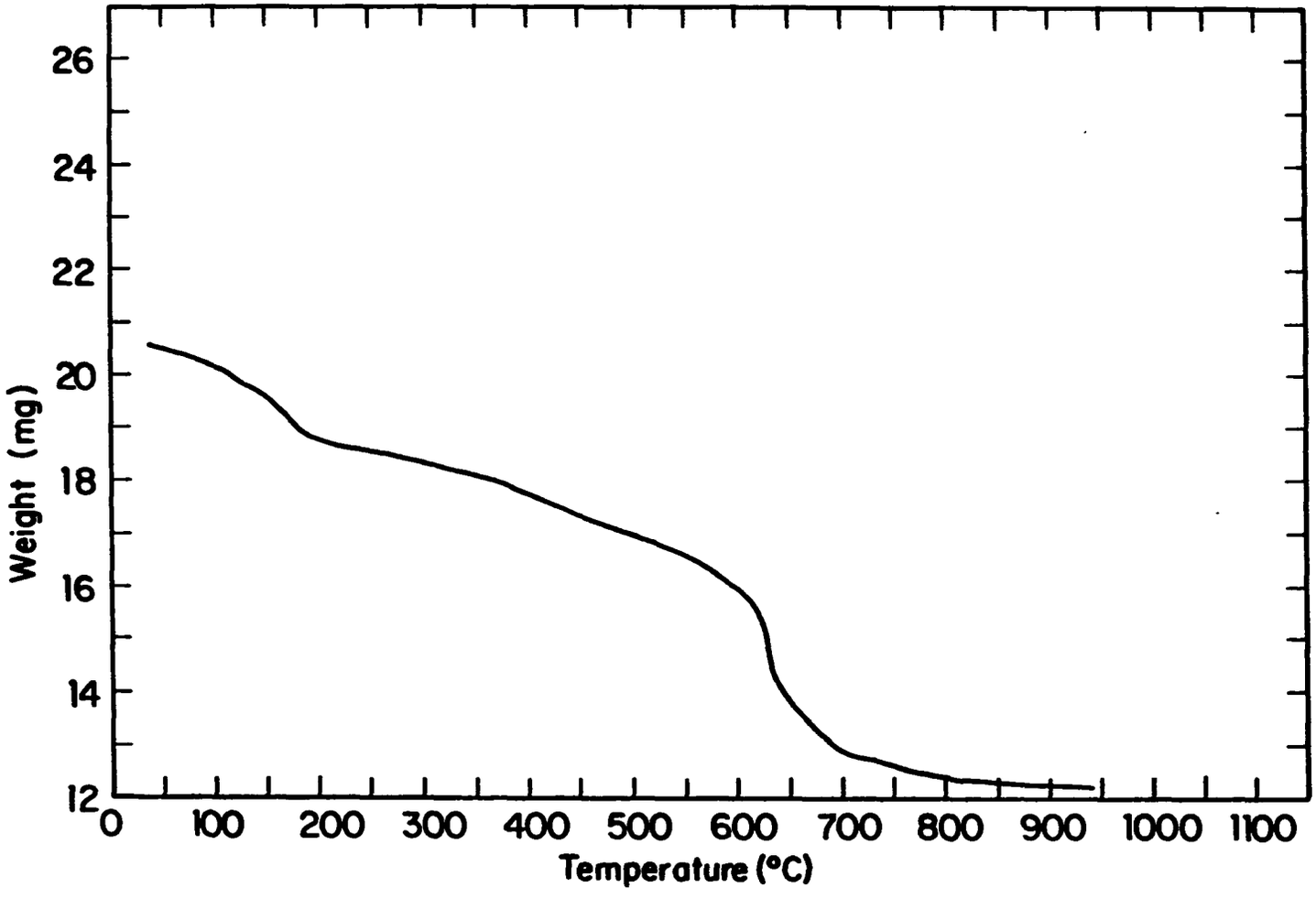

Figure 6. TGA curve for a powder from a precipitate prepared by reacting a solution 0.02 M in $Y(NO_3)_3$ and 0.25 M in urea for 1 hr. at 100°C. The heating rate was 10°C/min

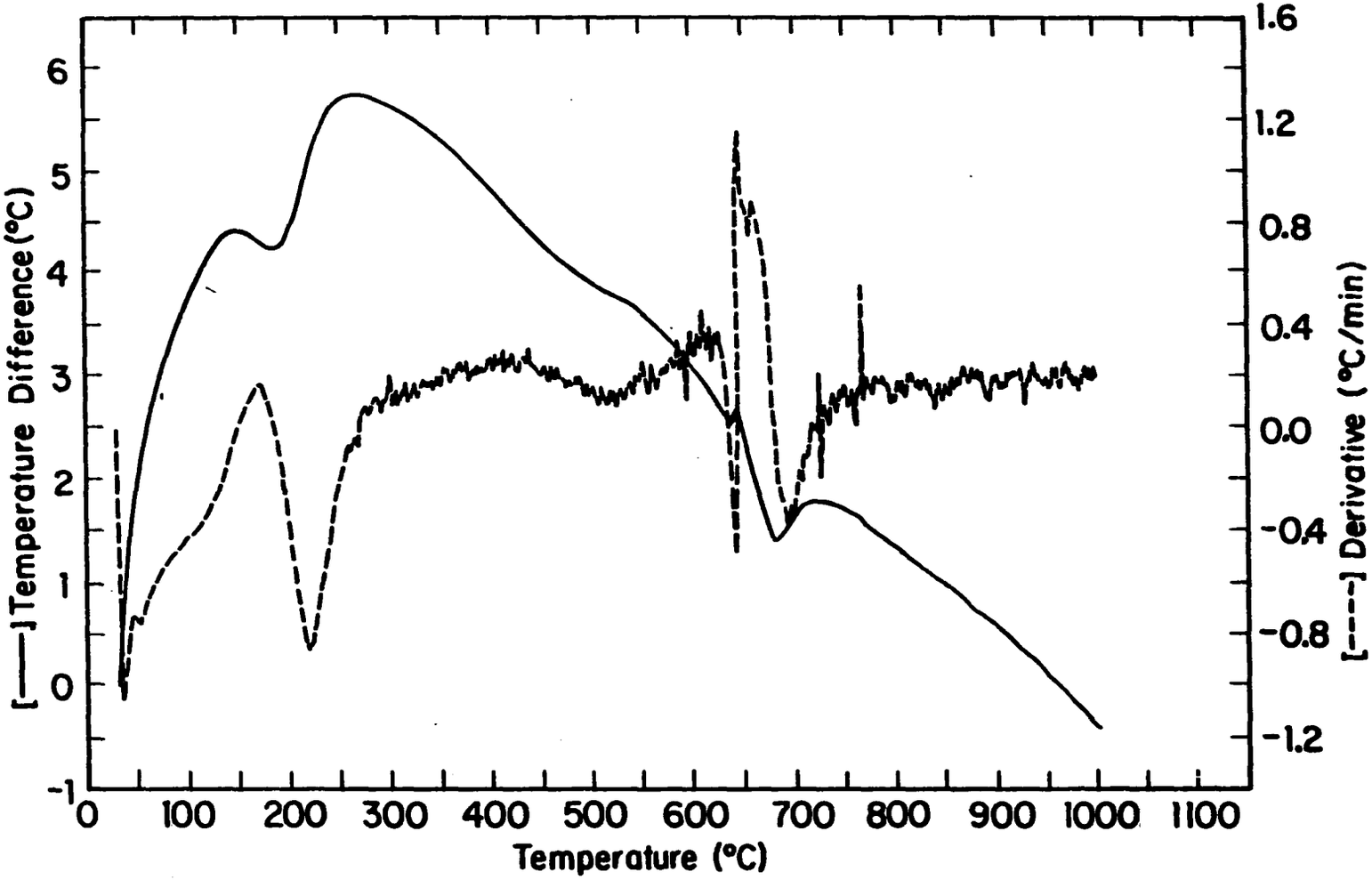

Figure 7. DTA curves for a powder as in Figure 6. The heating rate was 20°C/min.

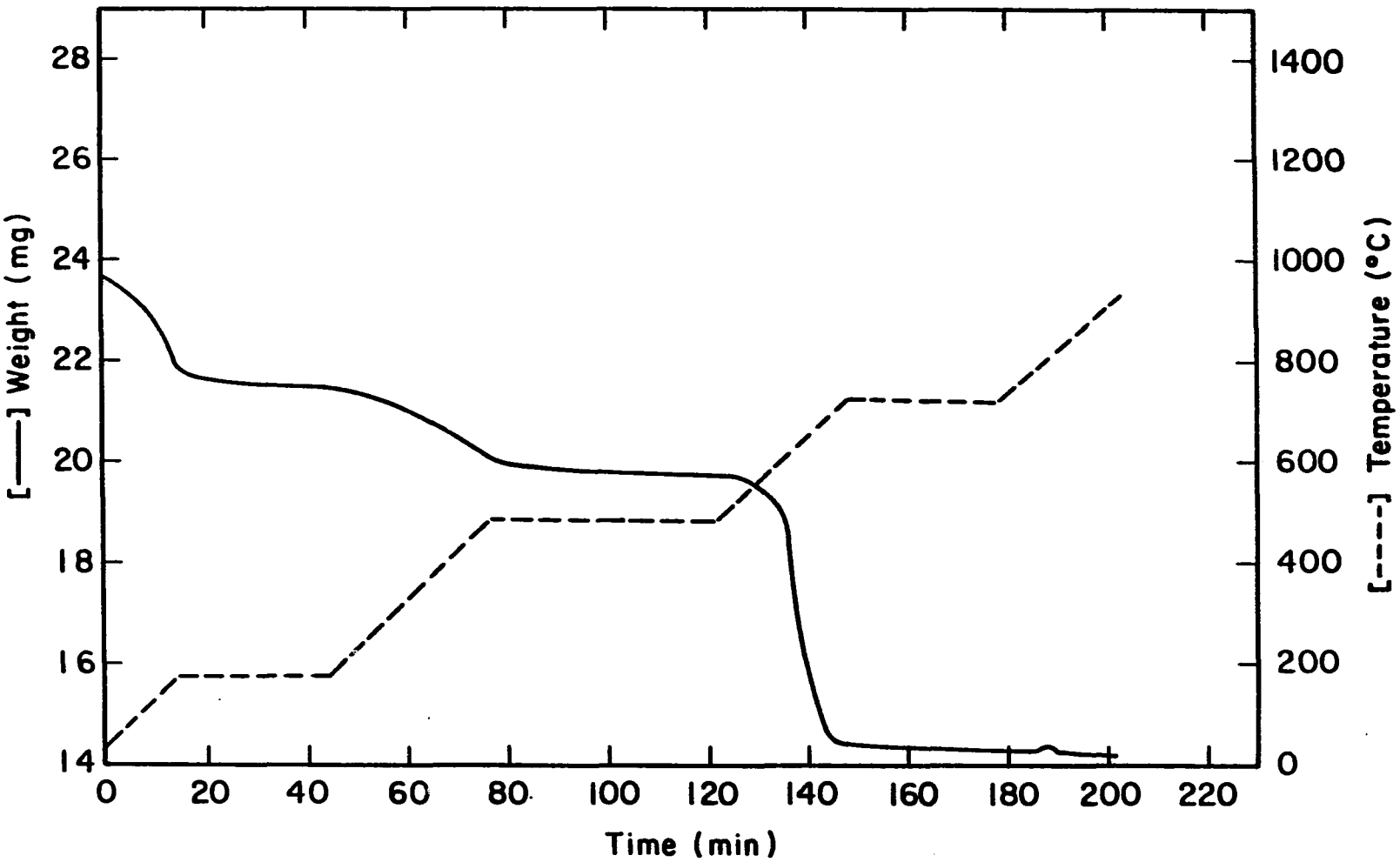

Figure 8. TGA curve obtained under both dynamic (10°C/min.) and static (at 185°C, 480°C, and 720°C) temperature conditions for a powder as in Figure 6.

temperatures (20°C - 1000°C), no nitrogen species were detected by the mass spectrometer; instead H_2O, OH, O_2, CO, and CO_2 species were observed. The carbon species dominated the high temperature region. Figures 9 and 10 show x-ray photoelectron spectra for the pre- and post-heated powders respectively. From the chemical analyses, the powders were found to contain 47% yttrium and 35% carbonate by weight.

The x-ray photoelectron spectrum of the pre-heated sample (Figure 9) indicates that the powder contains the elements Y, C, and O. However, the C-peak disappeared while the O-peak was reduced when the sample was heated to 1000°C (Figure 10). These results and the fact that no nitrogen species were detected in the gases that were given off as the powder was heated suggest that the compound contains neither urea nor a nitrate group. A presumption that the compound is yttrium hydroxy-carbonate with a composition $Y(OH)_{3-2x}(CO_3)_x.yH_2O$ and that when heated to 1000°C it changes to yttria is therefore not illogical.

The empirical formula that is consistent with results from thermal and chemical analyses is $Y(OH)CO_3.H_2O$. The first low temperature process (0°C - 200°C) is attributed to loss of water of hydration (or water adsorbed on the particle surfaces), the second process at intermediate temperatures (200°C - 600°C) to loss of structural water, and the third high temperature process (600°C - 1000°C) to loss of CO_2:

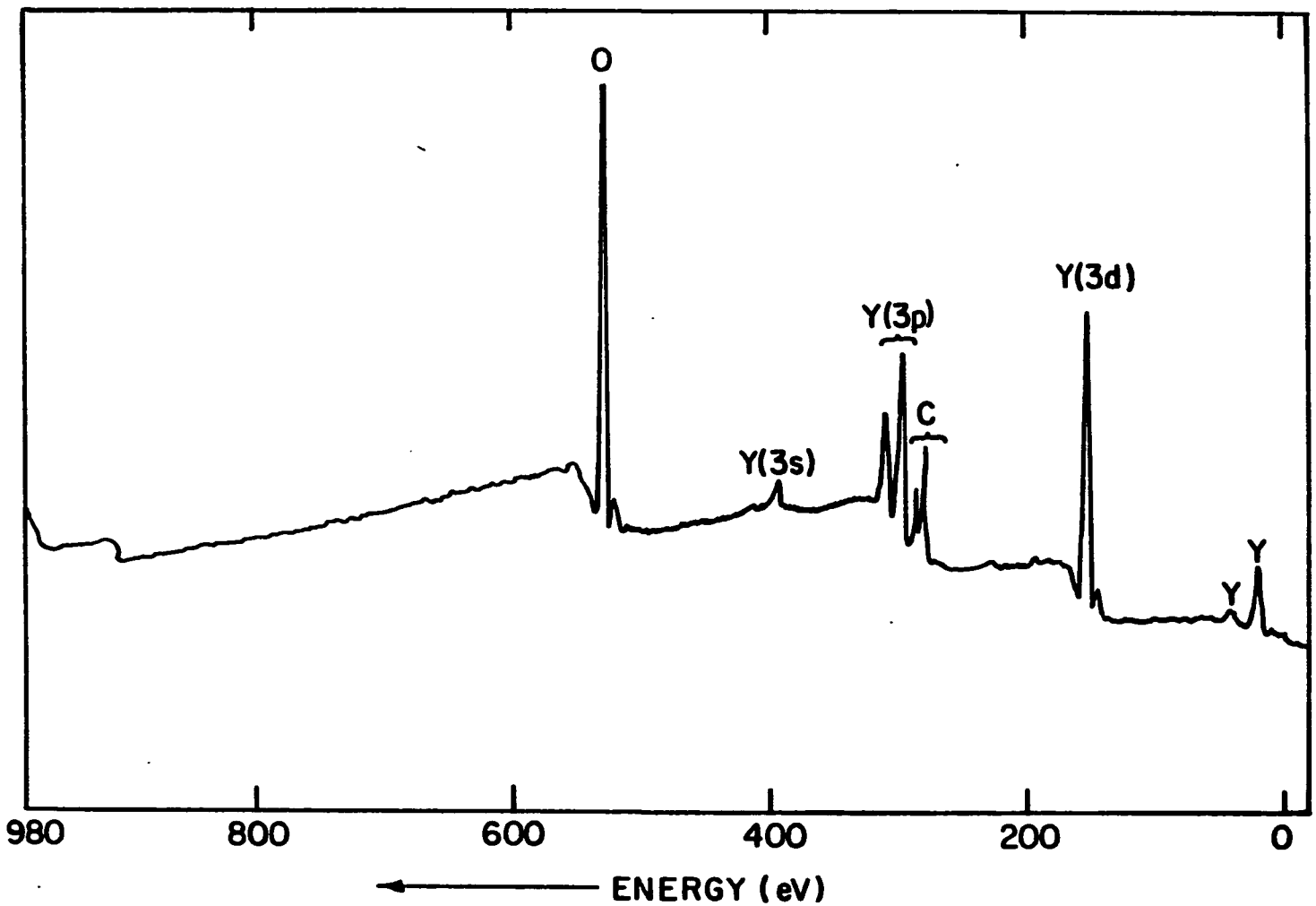

Figure 9. x-ray photoelectron spectrum of a powder as in Figure 6.

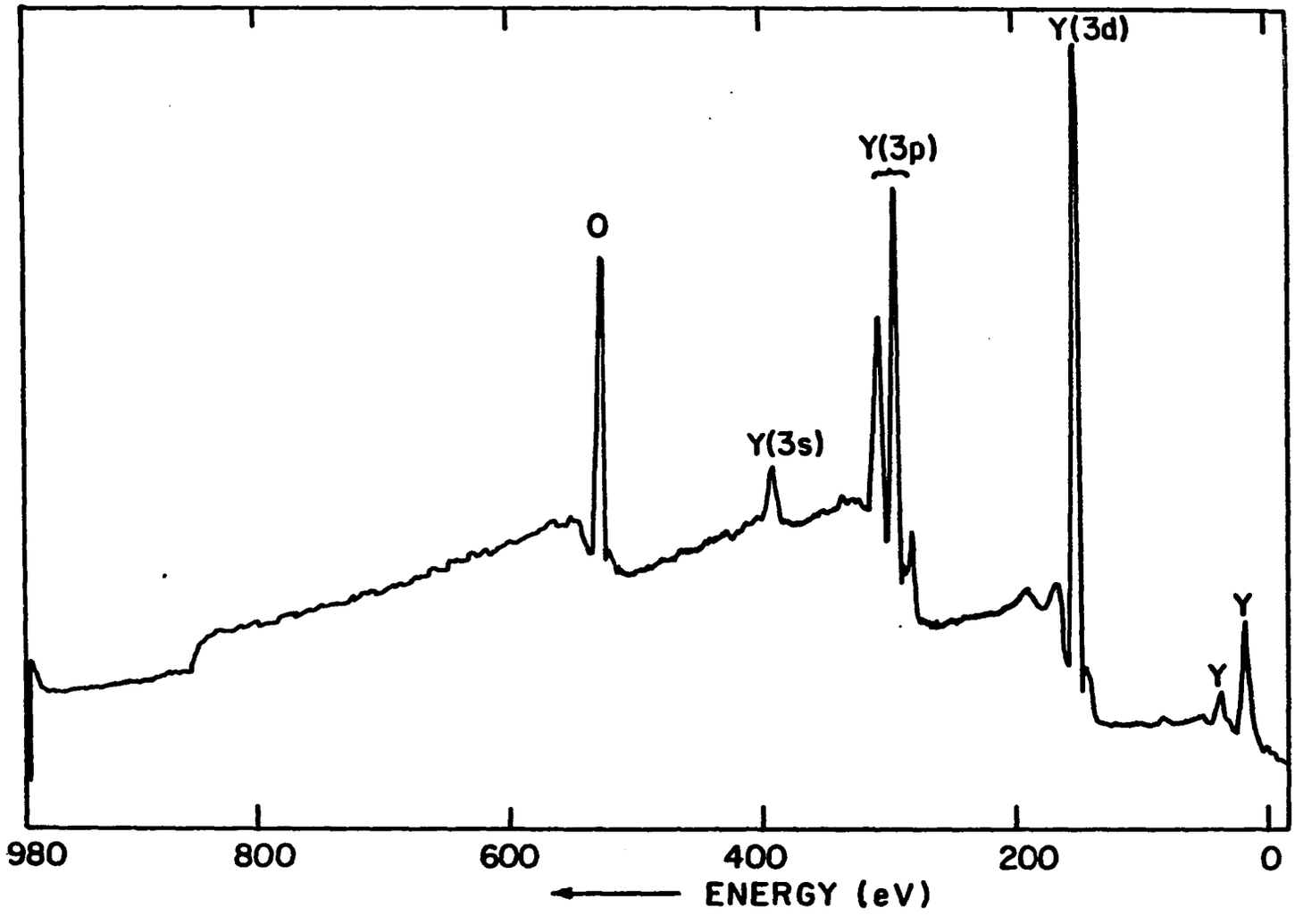

Figure 10. x-ray photoelectron spectrum of a powder (as in Figure 6) after being heated to 1000°C.

$$Y(OH)CO_3.H_2O \xrightarrow{20^o\text{-}200^oC} Y(OH)CO_3 + H_2O \quad [13]$$

$$2Y(OH)CO_3 \xrightarrow{200^o\text{-}600^oC} Y_2O(CO_3)_2 + H_2O \quad [14]$$

$$Y_2O(CO_3)_2 \xrightarrow{600^o\text{-}1000^oC} Y_2O_3 + 2CO_2 \quad [15]$$

Thus from chemical analyses, one observes per 100 gms, 47gms of Y, 35 gms of CO_3, and by difference 18 gms of $OH.H_2O$ corresponding to:
(47/88.9)=0.53 gm atoms of Y, (35/60)=0.58 gm "molecules" of CO_3, and (18/35)=0.51 gm "molecule" of $OH.H_2O$, while the analysis of the TGA results is presented in Table 3 below:

Table 3. Analysis of the TGA results of Figure 8

Compound	Wt./mg	Wt as % of 1	MW	MW as % of 1
1. $2Y(OH)CO_3 \cdot H_2O$	23.65	100	367.8	100
2. $2Y(OH)CO_3$	21.45	91	331.8	90
3. $Y_2O(CO_3)_2$	19.75	84	313.8	85
4. Y_2O_3	14.40	61	225.8	61

The transmission electron diffraction pattern of the powder shown in Figure 11 shows distinct but diffuse continuous rings suggesting that the material consists of small crystals with random orientation. Perfectly spherical but crystalline colloidal particles have been reported before (65-68). It is highly plausible that the spherical particles reported here are composed of crystallites of much smaller dimension. A more quantitative interpretation of Figure 11 is hampered by the limited number of rings obtained.

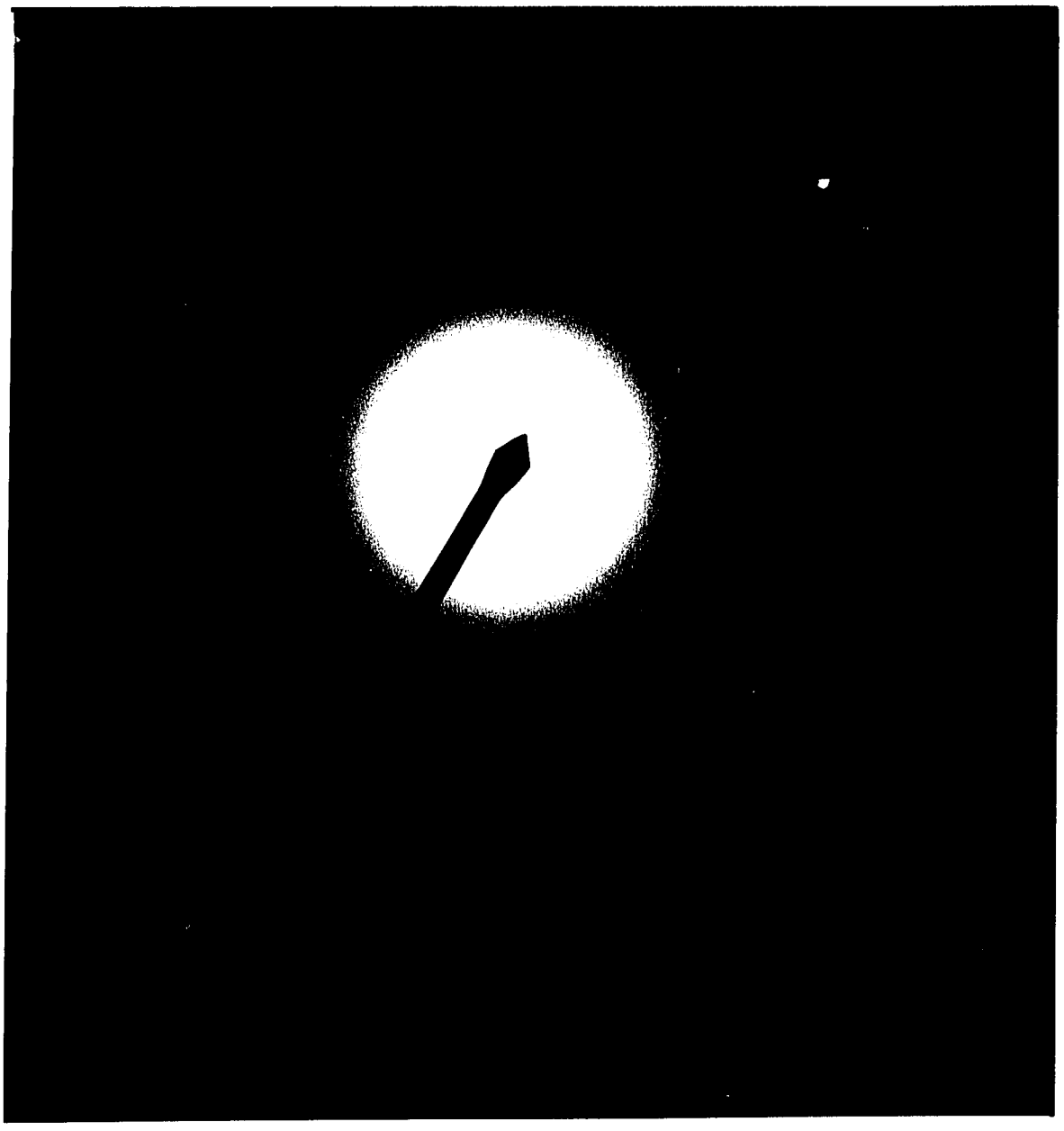

Figure 11. Transmission electron diffraction pattern of particles produced by reacting a solution 0.02 M in $Y(NO_3)_3$ and 0.25 M in urea for 5 minutes at 100°C. The accelerating voltage=120kV; the sample to photographic plate distance=46 cm.

B. Nucleation and Growth Studies

As stated earlier, the success in preparing monodisperse systems lies in the ability to arrange the formation of the precipitating material in such a way that all nucleation takes place in a very short period with additional material supplied so slowly, that it can find its way to the nuclei without the supersaturation reaching a level at which further nucleation could occur. LaMer and Dinegar (69) expressed this situation in a simple diagram (Figure 12) relating to their preparation of sulfur sols from acidified thiosulfate. The concentration of the precipitating material (sulfur in the case of LaMer and Dinegar) formed by the chemical reaction increases with time until it reaches a critical supersaturation (the nucleation concentration, C_n), when nucleation occurs. This condition results in the formation of many nuclei in a short burst. They grow rapidly, which lowers the concentration to a value below the nucleation concentration, but high enough to allow particle growth to occur at a rate that just consumes all further material that is generated.

The induction period, τ measured can, for the sake of simplicity, be taken as the induction time for nucleation. Strictly though, it includes the nucleation period and the time for growth of the particles to a size large enough for visible turbidity.

Plots of ln $1/\tau$ versus (i) ln [urea], (ii) ln $[H^+]$, and (iii) ln $[Y(NO_3)_3]$, where [urea], $[H^+]$, and $[Y(NO_3)_3]$ are

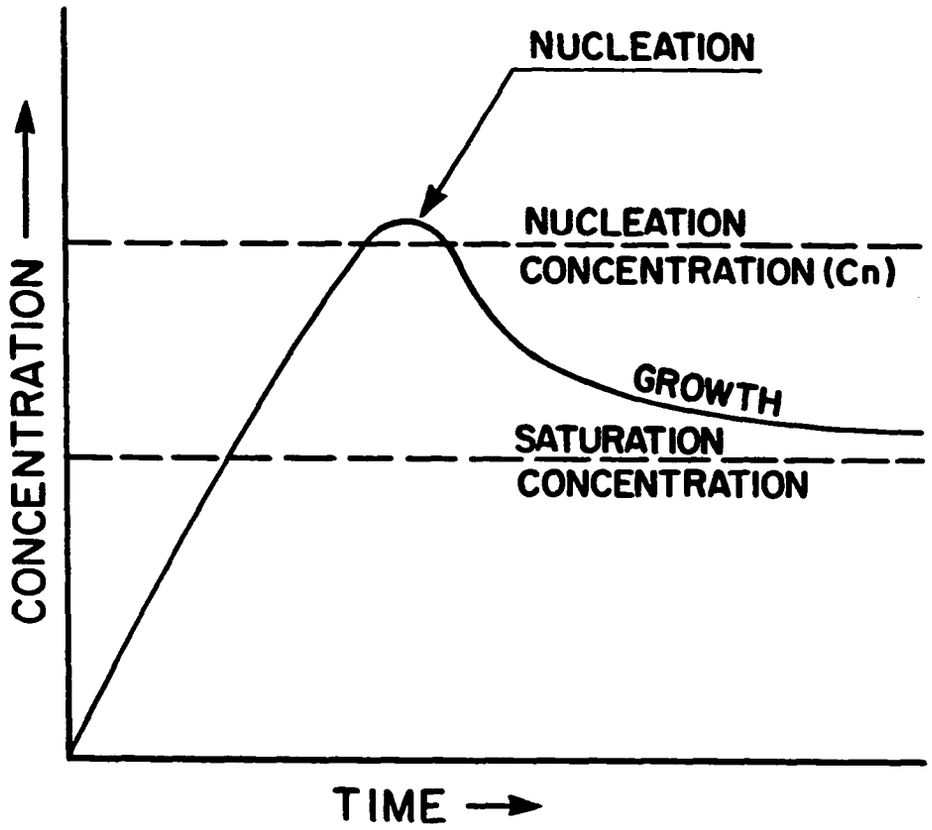

Figure 12. Illustrating the formation of a monodisperse system by controlled nucleation and growth

initial concentrations, were linear with slopes of 0.9, -0.8, and -0.02 respectively (Figure 13). These results can be simply explained if the following are assumed:

(i) no precipitating species are formed until the initial acidity has been neutralized

(ii) the reaction between yttrium ions and the hydrolysis products of urea is much faster than the decomposition of urea. Hence, the decomposition of urea is rate-limiting

(iii) the solubility of the precipitate is so low that for all practical purposes it (the precipitate) can be regarded as insoluble

Let C_h be the initial hydrogen ion concentration, C_o the initial urea concentration, and suppose that 'a' equivalents of H^+ are neutralized per mole of urea decomposed. Decomposition of urea is first order; let k be the first order rate constant for urea decomposition. Then the time t_o for complete neutralization of acid is related to C_h and C_o by:

$$C_h = aC_o\,(1-e^{-kt_o}) \qquad [16]$$

But k is of the order of 10^{-5} sec^{-1} (APPENDIX A) and the maximum reaction time (t_{max}) for our experiments was 30 minutes.

Therefore, $(kt_o)_{max} = 0.018$

Thus replacing $(1-e^{-kt_o})$ by kt_o creates a maximum error of only 0.9%.

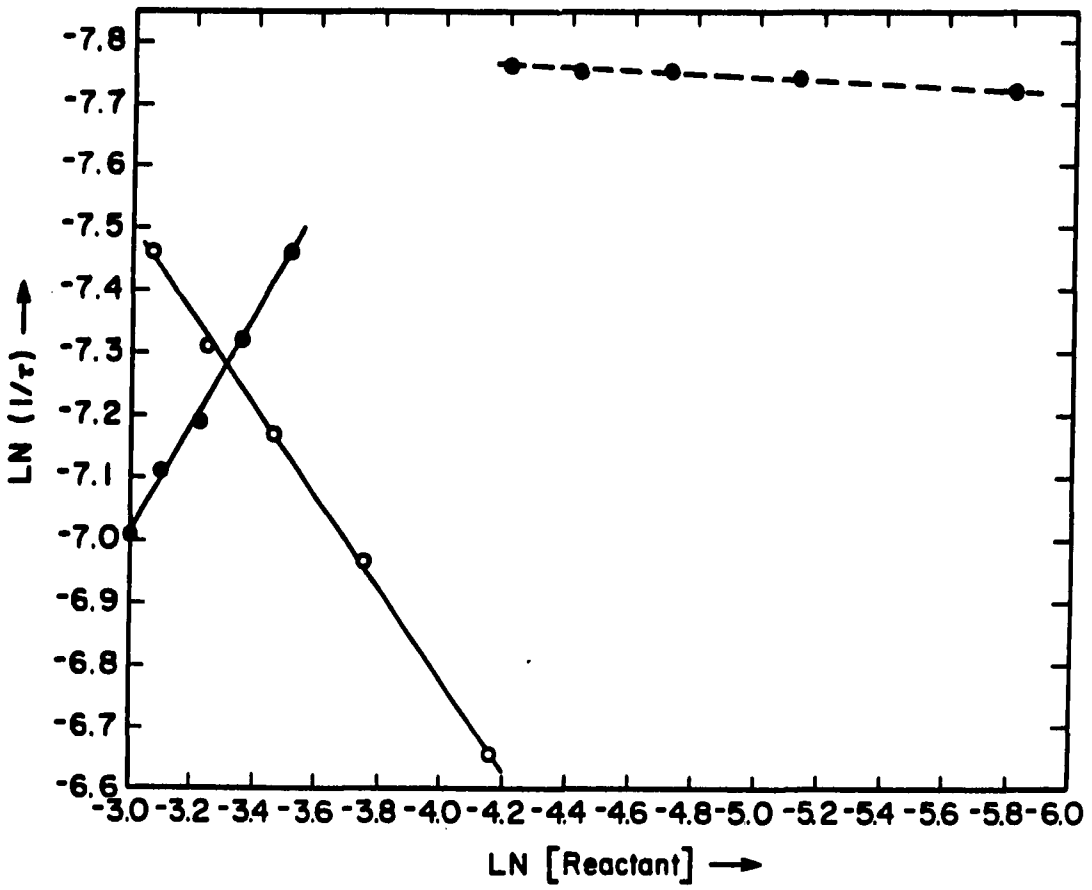

Figure 13. Ln $1/\tau$ versus: (i) ln [urea] (●—●—●). $[Y(NO_3)_3]$=0.05 M, $[HNO_3]$=0.078 M, temperature=100°C, and slope=0.9 (ii) ln $[H^+]$ (○—○—○). $[Y(NO_3)_3]$=0.05 M, [urea]=0.5 M, temperature=100°C, and slope=-0.8 (iii) ln $[Y(NO_3)_3]$ (●- -●- -●). [urea]=0.5 M, $[HNO_3]$=0.078 M, temperature=100°C, and slope=-0.02

Therefore $$t_o \propto \frac{C_h}{aC_ok} \quad [17]$$

At t_o, when the precipitating species begin to form, the remaining concentration of urea is $C_oe^{-kt_o}$.

If b is the number of moles of precipitating material formed for every mole of urea that reacts:

$$C_p = bC_oe^{-kt_o}(1-e^{-k(t-t_o)}) \simeq bC_oe^{-kt_o}k(t-t_o) \quad [18]$$

C_p is the concentration of precipitating species at time t. The maximum error in replacing e^{-kt_o} by $1-kt_o$ is only 0.01%, hence:

$$C_p = bC_ok(1-kt_o)(t-t_o) \quad [19]$$

But recall that at $t=\tau$, $C_p=C_n$

$$C_n = bC_ok(1-kt_o)(\tau-t_o) \quad [20]$$

or $$\frac{1}{\tau} = \frac{(1-kt_o)}{[(C_n/bC_ok) + t_o(1-kt_o)]} \quad [21]$$

From assumption (iii) and if the nucleation concentration (C_n) is not much higher than the saturation concentration, then:

$C_n << bC_ok$

So $$\frac{C_n}{bC_ok} << t_o(1-kt_o) \quad [22]$$

Thus, $\tau=t_o$

Substituting τ for t_o in equation [17], and rearranging:

$$\frac{1}{\tau} = \frac{aC_ok}{C_h} \quad [23]$$

From results of pH measurements plotted in Figure 14, the amount of H^+ present in solutions of various compositions (i.e., urea: $Y(NO_3)_3$) but containing no HNO_3 can be determined. It follows that in all studied systems containing HNO_3, the amount of H^+ from HNO_3 far outweighs that from solutions containing no HNO_3 of otherwise similar compositions. Consequently, HNO_3 can be regarded as the sole source of all the H^+ in such systems.

It is not surprising, therefore, that plots of ln $1/\tau$ versus ln [urea], ln $[H^+]$, and ln $[Y(NO_3)_3]$ were linear with slopes close to those expected of 1, -1 and 0 respectively. Discrepancies can be attributed to the oversimplification in the treatment of induction period, the approximations made, and inevitable experimental errors.

Nucleation ensues once the concentration of the precipitating material reaches the nucleation concentration, followed by particle growth as shown in Figure 15. A standard model of steady-state diffusion controlled growth of a colloidal particle leads to a capture rate, Q (moles/particle sec) which depends on the diffusion coefficient, D (cm^2/sec), concentration of diffusant, C (moles/cm^3), and particle radius, r (cm) according to:

$$Q = 4\pi DCr \qquad [24]$$

If the particle grows by a volume, $\bar{V}$ (cm^3/mole) per mole of diffusant captured, we have:

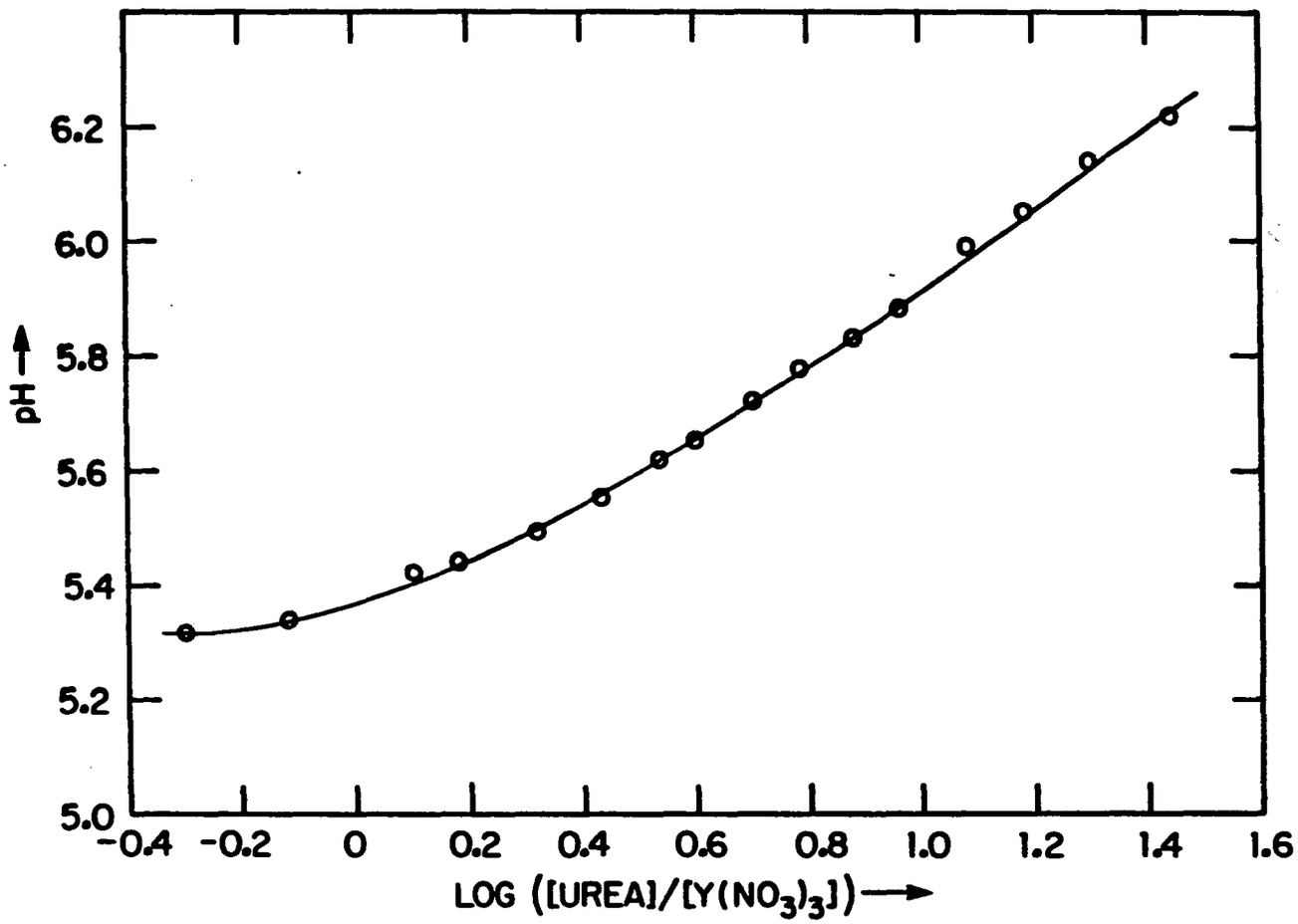

Figure 14. PH versus log ([urea]/[$Y(NO_3)_3$]) for solutions containing different urea to $Y(NO_3)_3$ ratios

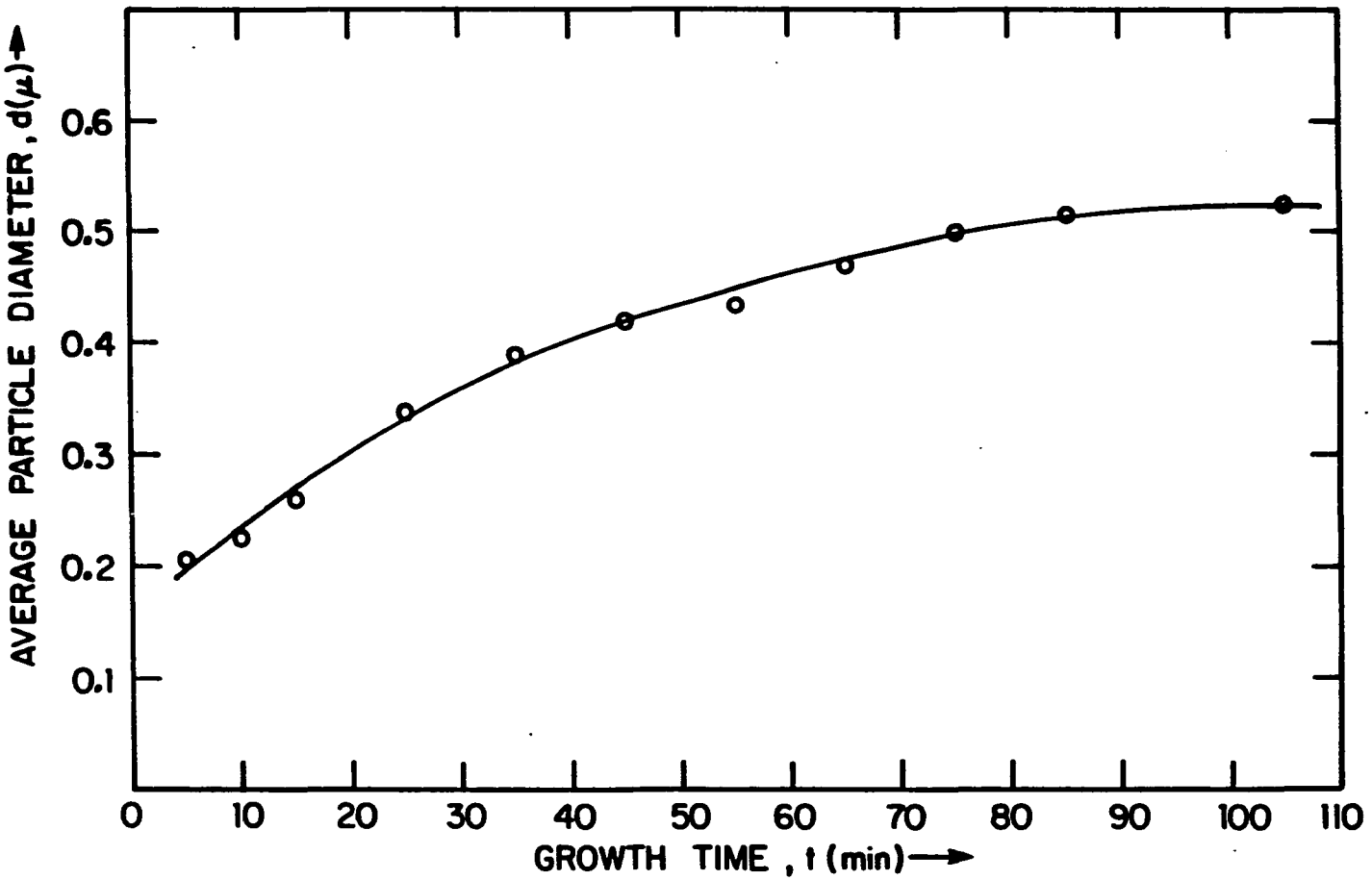

Figure 15. Average diameter versus growth time for particles obtained by reacting a solution 0.02 M in $Y(NO_3)_3$ and 0.25 M in urea at 100°C

$$4\pi r^2 \frac{dr}{dt} = Q\bar{V} = 4\pi DCr\bar{V} \qquad [25]$$

or

$$r \frac{dr}{dt} = DC\bar{V} \qquad [26]$$

If C is constant, this can immediately be integrated to obtain:

$$r^2 = r_o^2 + 2DC\bar{V}t \qquad [27]$$

where r_o is the initial particle radius.

or

$$d^2 = d_o^2 + 8DC\bar{V}t \qquad [28]$$

where $d = 2r$ is the particle diameter.

An equivalent result was used by LaMer and Dinegar (70).

In the present case, the concentration, C may be changing as a result of the decomposition reactions producing the diffusant. We consider a model in which n particles per cm^3, of radius r_o are immersed in a solution of decomposable species, A of initial concentration, X_o and assume:

(i) the particles grow by diffusion of single molecules to the surfaces of these particles, where they "condense" without change

(ii) the diffusing molecules B are formed by first-order decomposition of species A, concentration X, initial concentration Xo, and decomposition first-order rate constant k

(iii) b moles of B are produced per mole of A that decomposes

(iv) the transients can be ignored

The concentration, C in equation [26] is now understood to mean that of the diffusant B. By assumptions (ii) and (iii), after time t there will have been produced $bX_o(1-e^{-kt})$ moles/cm^3 of B, of which by asssumption (i) $4\pi n(r^3-r_o^3)/3\bar{V}$ will have been consumed in the growth of particles. Assuming C=0 at t=0, we have:

$$C = bX_o(1-e^{-kt}) - \frac{4\pi n(r^3-r_o^3)}{3\bar{V}} \qquad [29]$$

Substituting in equation [26] and rearranging, we obtain:

$$r\frac{dr}{dt} + \frac{4\pi nD(r^3-r_o^3)}{3} = bX_oD\bar{V}(1-e^{-kt}) \qquad [30]$$

For reasons given following equation [16], we replace $(1-e^{-kt})$ by kt, and we also neglect r(dr/dt) as a zeroth approximation whose validity is to be subsequently confirmed. Then:

$$r^3 = r_o^3 + \frac{3bX_o\bar{V}kt}{4\pi n} \qquad [31]$$

or

$$d^3 = d_o^3 + \frac{6bX_o\bar{V}kt}{\pi n} \qquad [32]$$

From [31], in zeroth approximation:

$$r\frac{dr}{dt} = \frac{bX_o\bar{V}k}{4\pi nr} \qquad [33]$$

This is small compared to $bX_oD\bar{V}kt$, justifying the zeroth order approximation, if $4\pi nrDt>>1$. In the experiments being considered, $n>10^{10}$ particles/cm^3, $r>10^{-5}$ cm, $D\sim10^{-5}$ cm^2/sec, and $t>240$sec, so $4\pi nrDt>3000$. It should be noted, that neglect of $r(dr/dt)$ in equation [30] is equivalent to neglect of C in equation [29], implying that the material produced by decomposition of A is largely consumed by precipitation. Having justified the zeroth approximation, we can use equation [33] in equation [26] to obtain a good approximation to C:

$$C = \frac{bX_ok}{4\pi nrD} \qquad [34]$$

The free concentration hence decreases as the radius increases so that the total rate of capture $4\pi nrDC$ equals the rate of production of B, bX_ok, which is constant over the time period for which the assumption $kt<<1$ is justified. According to equation [28], a plot of d^2 versus t should be linear with intercept d_o^2 and slope $8DC\bar{V}$, while according to equation [32] a plot of d^3 versus t should be linear with intercept d_o^3 and slope $(6bX_o\bar{V}k)/\pi n$. These plots are compared in Figure 16.

It is clear that our data fit equation [32] but not [28], indicating that the free concentration of the diffusant decreases with particle growth. The obtained intercept of about zero is reasonable since nuclei are normally of the order of 20Å in diameter, while the

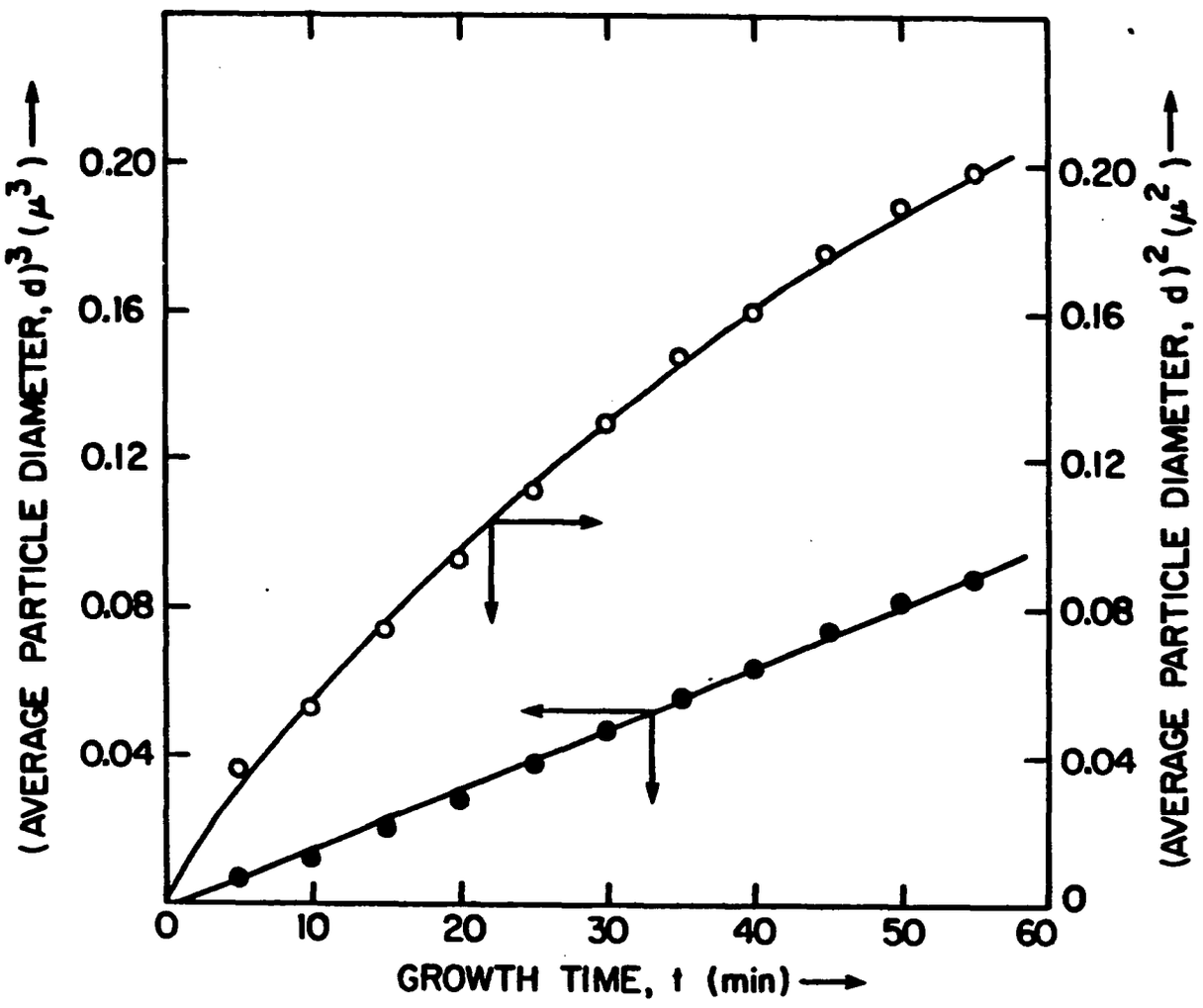

Figure 16. Plots of (i) (average particle diameter)^2 (-o-o-o-) and (ii) (average particle diameter)^3 (-●-●-●-) versus growth time from the data of figure 15. The slope of (ii) = $1.78 \times 10^{-3} \mu^3$/min

reasonableness of the slope is to be subsequently proved through determination of the number of particles per cm^3, n. The narrowing of the particle size distribution with growth time, as shown in Figure 17, is also characteristic of diffusion-controlled growth.

If precipitation does not take place until the initial acidity is neutralized, it is highly possible that both hydrolysis reactions of urea at neutral conditions do proceed simultaneously:

$$CO(NH_2)_2 + 2H_2O \longrightarrow 2NH_4^+ + CO_3^{2-} \quad [35]$$

$$CO(NH_2)_2 + 3H_2O \longrightarrow 2NH_4^+ + 2OH^- + CO_2 \quad [36]$$

Assuming that:

(i) all the CO_3^{2-} come from reaction [35] (i.e. neglecting any CO_3^{2-}/HCO_3^- from CO_2 solubility)

(ii) all the OH^- produced by reaction [36] are consumed by the Y^{3+}

(iii) urea splits between reactions [35] and [36] in the ratio $\alpha:\beta$ when it decomposes

then the following reactions take place when $\alpha+\beta$ moles of urea hydrolyze:

$$\alpha CO(NH_2)_2 + 2\alpha H_2O \longrightarrow 2\alpha NH_4^+ + \alpha CO_3^{2-} \quad [37]$$

$$\beta CO(NH_2)_2 + 3\beta H_2O \longrightarrow 2\beta NH_4^+ + 2\beta OH^- + \beta CO_2 \quad [38]$$

$$((2\alpha+2\beta)/3)Y^{3+} + 2\beta OH^- + \alpha CO_3^{2-} \longrightarrow Y_{((2\alpha+2\beta)/3)}(OH)_{2\beta}(CO_3)_\alpha \quad [39]$$

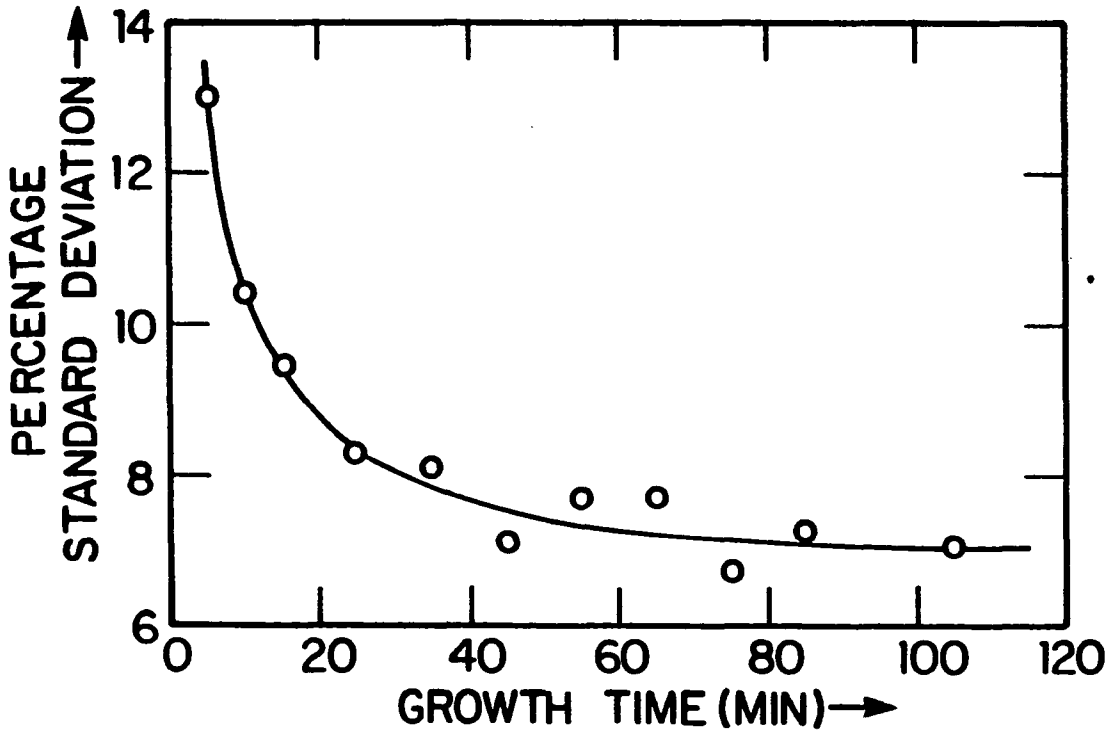

Figure 17. Percentage standard deviation of the size distribution as a function of growth time for particles as in Figure 15.

The overall reaction is:

$$(\alpha+\beta)CO(NH_2)_2 + (2\alpha+3\beta)H_2O + ((2\alpha+2\beta)/3)Y^{3+}$$

$$\longrightarrow Y_{((2\alpha+2\beta)/3)}(OH)_{2\beta}(CO_3)_{\alpha} + (2\alpha+2\beta)NH_4^{+} + \beta CO_2 \quad [40]$$

Therefore, for every mole of urea that decomposes, $1/(\alpha+\beta)$ moles of precipitating species are produced. This is equivalent to b in equation [32].

A plot of d^3 versus t (Figure 16) had a slope of $1.78X10^{-3}\mu^3$/min. (or $2.96X10^{-17}cm^3/s$).

For a precipitate of composition $Y(OH)CO_3$ and density $2.17g/cm^3$, $\alpha=1$ and $\beta=0.5 \rightarrow b=1/1.5$

$X_o = 0.25M$ (or $2.5X10^{-4}moles/cm^3$)

$\bar{V}$ = (molar mass/density) = $166/2.17 = 76.5cm^3/mole$

$k = 3.80X10^{-5}sec^{-1}$; using the value of Shaw and Bordeaux (61). Also see APPENDIX A.

$n = (6bX_o\bar{V}k/\pi.slope) = 3X10^{10}$ particles/cm^3

Therefore, the nucleation event produced $3X10^{10}$ particles/cm^3. It is interesting to note that Jean and Ring (71), in their study of the nucleation and growth phenomena generating monosized TiO_2 powders by the hydrolysis of $Ti(OC_2H_5)_4$ in ethanol solution, found that the nucleation event produced between $4X10^9$ and $11X10^{10}$ particles/cm^3.

The diffusion chronomal analysis (72) was applied to the data of Figure 15. This chronomal is defined as:

$$I_D = \int_0^{\alpha_D} x^{-1/3}(1-x)^{-1}dx \quad [41]$$

$$= \frac{1}{2}\ln\frac{(1-\alpha_D)}{(1-\alpha_D^{1/3})^3} - \sqrt{3}\tan^{-1}\frac{\sqrt{3}}{1+2\alpha_D^{-1/3}} \quad [42]$$

α_D is the fraction of diffusing species which has reacted to form the precipitate at time t. For the period where the greater part of the change in α_D takes place, a good approximation is:

$$\alpha_D = \{d(t)/d_o\}^3 \qquad [43]$$

d(t) is the particle diameter at time t, while d_o is the limiting diameter.

t is related to the chronomal I_D according to:

$$t = K_D I_D \qquad [44]$$

where

$$K_D = \frac{d_o^2}{12 V_m D C_m} \qquad [45]$$

V_m and D are the molecular volume and diffusion coefficient of the diffusing species respectively, while C_m is the total concentration of the diffusing species produced throughout the entire growth period. Taking the limiting diameter, d_o as 0.525μ (corresponding to approximately 105 min. after the end of induction period), a plot of I_D versus t was linear (Figure 18), supporting the diffusion-controlled mechanism of particle growth.

The induction periods and average particle diameters obtained from silica seeded precipitation experiments are plotted as functions of log N_C (where N_C is the number of silica seeds/cm^3) in Figure 19. In systems with $N_C \geq 4X10^{10}$ (equivalent to log N_C of 10.6), it was observed that the increase in turbidity of the sols with time during the reaction was gradual while in systems with $N_C < 4X10^{10}$, the turbidity intensified rather rapidly.

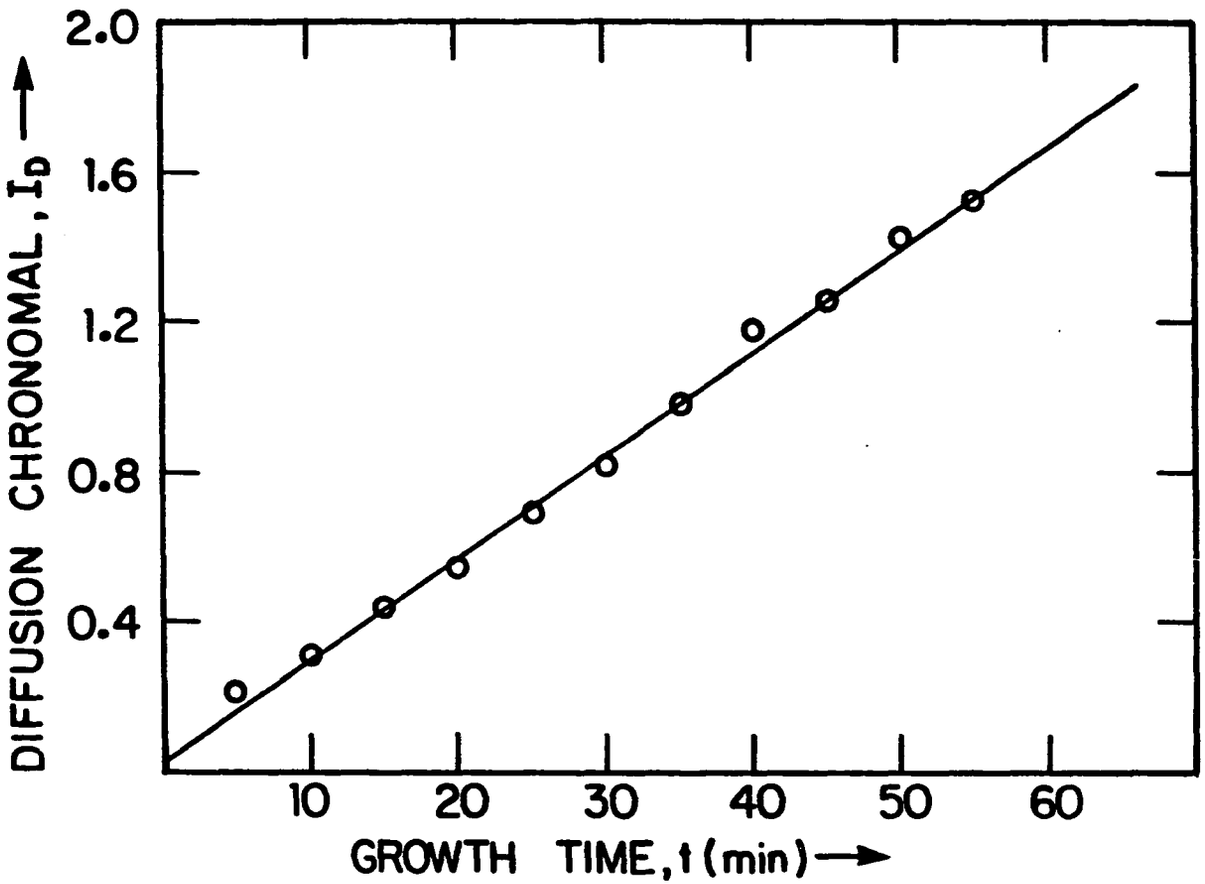

Figure 18. The diffusion chronomal versus growth time from the data of Figure 15.

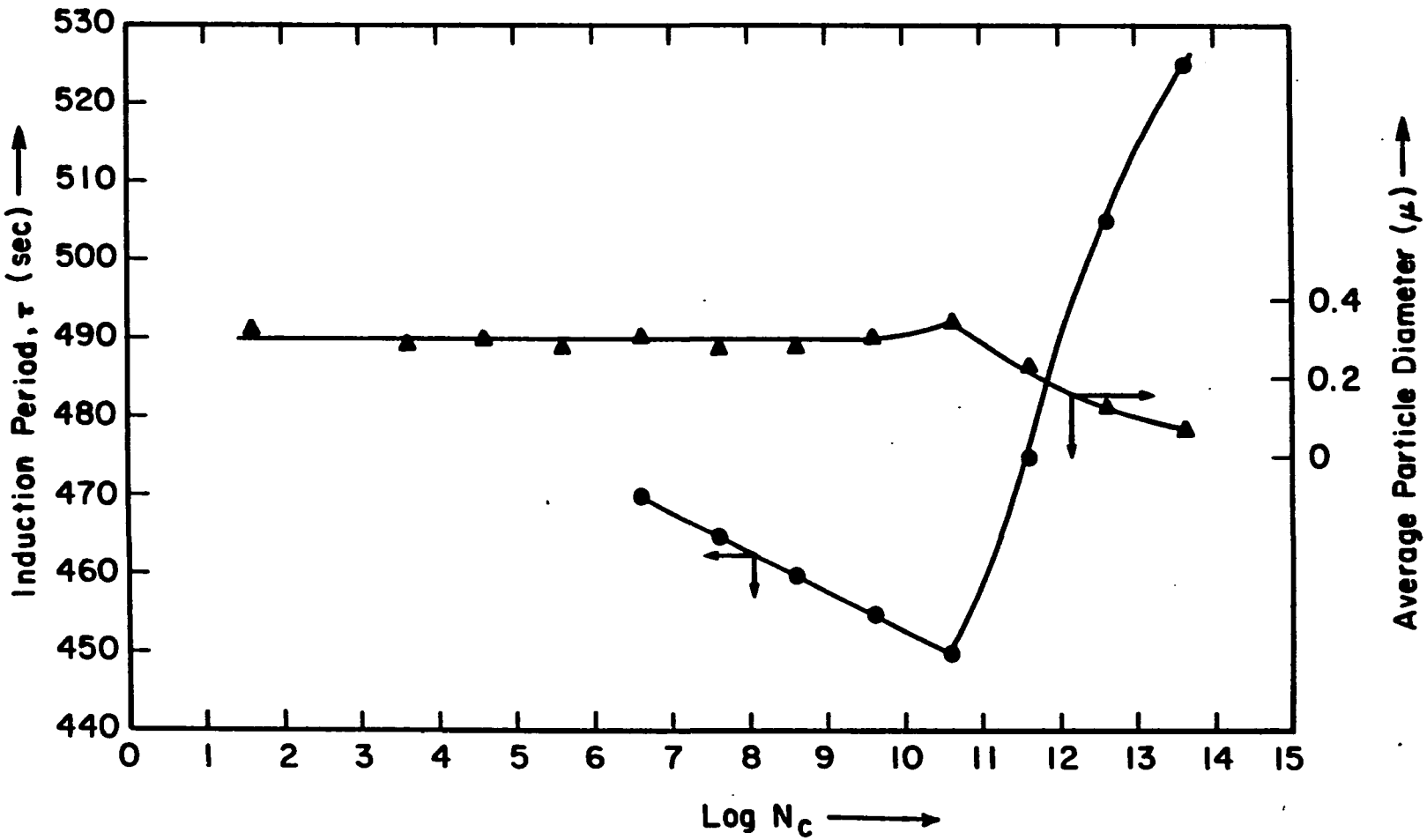

Figure 19. The effect of varying the number of silica seeds, N_c in a solution 0.05 M in $Y(NO_3)_3$ and 0.24 M in urea reacted at 100°C for 35 minutes on the induction period (-●-●-●-) and average particle diameter (-▲-▲-▲-)

It appears that in systems with $N_C \geq 4X10^{10}$, the seeds are so abundant that they resist the supersaturation of the precipitating species in solution from building up to levels necessary for homogeneous nucleation. Hence, either heterogeneous nucleation followed by growth or pure growth onto the silica seeds ensues. Whatever the mechanism might be, it would be expected that the system with most seeds would have the smallest overall particles as a consequence of tremendous material distribution among the seeds. Although turbidity is a function of both particle number density and size, as given by the equation below (73):

$$T = N_C K_m \pi r^2 \qquad [46]$$

where T is the turbidity, K_m is the Mie scattering coefficient, and r is the particle radius, it seems that the predominant factor in these systems is particle size. Again as a result of material distribution, the particles in the system with the least number of seeds would be expected most quickly to reach the critical size (call r_τ) corresponding to the minimum visible turbidity. Consequently, such a system would have the shortest induction period.

The $4X10^{10}$ seems to be the critical number concentration (CNC) of silica seeds below which pure heterogeneous precipitation cannot occur. A plausible explanation for this is that below this value, the seeds are too few to adequately relieve the concentration of precipitating species and hence cannot impede the concentration build-up

to the critical supersaturation value necessary for homogeneous nucleation. It is interesting to note that the CNC value is almost the same as the number concentration of particles found to be produced in non-seeded precipitating systems of $3X10^{10}$ particles/cm^3. In fact, it appears that in systems with $N_c < 4X10^{10}$, homogeneous nucleation takes place yielding enough nuclei to bring the total number of concentration of particles close to the CNC value. The overall size of the particles in all these systems would be expected to be the same. The system with the least number of seeds will produce a lot more nuclei than the existing seeds and therefore the induction period will depend on the time required for these nuclei to reach r_τ. In contrast, the system with most seeds will produce negligibly few nuclei compared to the existing seeds and therefore the induction period will depend on the time needed for the seeds to reach r_τ. The induction period for the latter system will be shorter. It should be stressed that in these systems (i.e., with $N_c < 4X10^{10}$), homogeneous nucleation is always preceded by heterogeneous precipitation, and that for induction period interpretations, both the number density and size factors must be taken into consideration.

Since no method has yet been found that entirely eliminates impurities from aqueous solutions, it is reasonable to say that in all systems there is a fair number of impurity particles in addition to the silica seeds

intentionally introduced into the systems. The explanation given above still holds whether this number, which is expected to be pretty much the same in all systems, is taken into consideration or not.

Particles from systems with $N_c < 4X10^{10}$ were more polydispersed than those from systems with $Nc \geq 4X10^{10}$ (compare Figures 20 (a) and (b) with (c)). This lends support to the fact that new nuclei were formed in systems with $N_c < 4X10^{10}$. On the other hand, this polydispersity is moderated by the fact that these particles grow by diffusion.

C. Stability of Sols and Order Packing

The sols used in this study comprised of particles (shown in Figure 21) with an average radius of 0.21μ. Using the classical sedimentation velocity equation [12], the sedimentation velocity (V) of these particles in water at 20^{o}C is 0.4 mm/hr. Such a low settling rate is compensated for by random convection currents making the sol stable with respect to sedimentation.

A plot of dA/dt versus pH is shown in Figure 22. Maximum flocculation is obtained at a pH of about 7.7. This behavior is expected since this pH is in the region of the point of zero net charge (or IEP). On either side of this pH, stability picks up sharply due to surface charging, with excellent stability being achieved in the pH range of 8.4

(a)

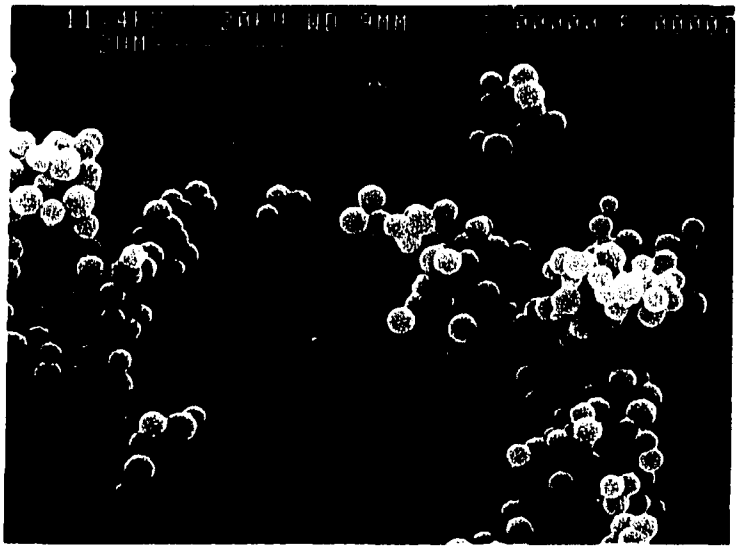

(b)

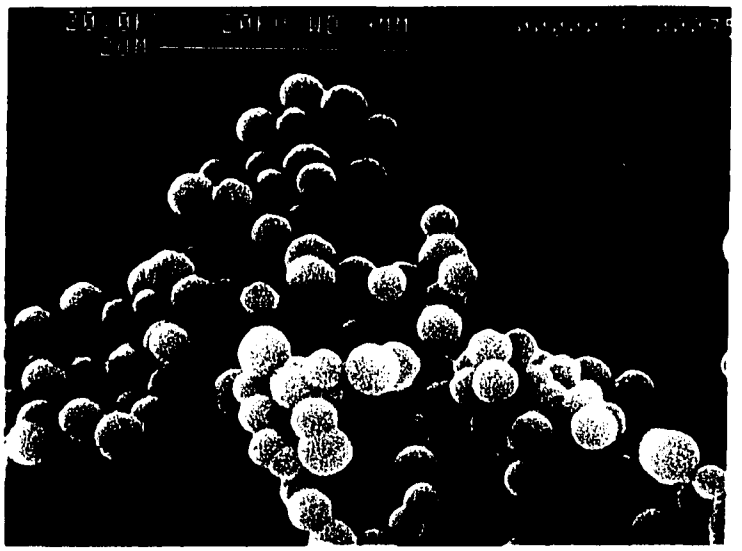

Figure 20. SEMs of particles obtained by heating solutions containing 0.05 M $Y(NO_3)_3$, 0.24 M urea, and (a) $4X10^6$ and (b) $4X10^8$ silica seeds/cm^3, at 100°C for 35 minutes

(c)

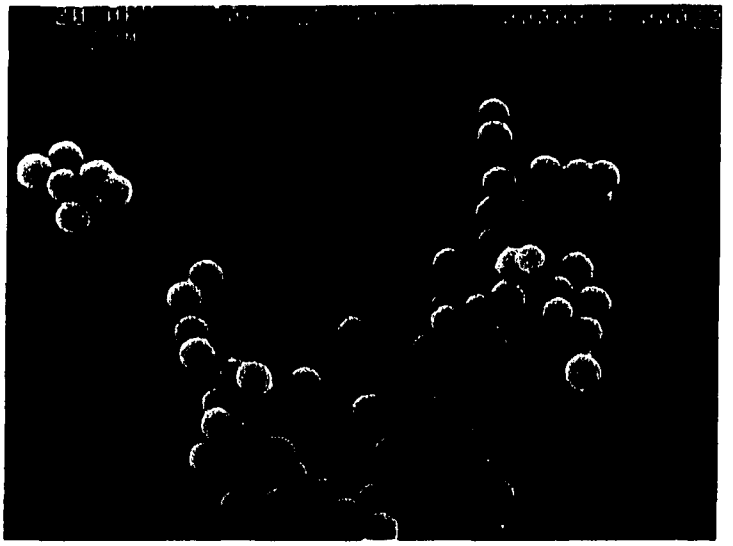

Figure 20. (continued)
(c) $4X10^{11}$ silica seeds/cm^3

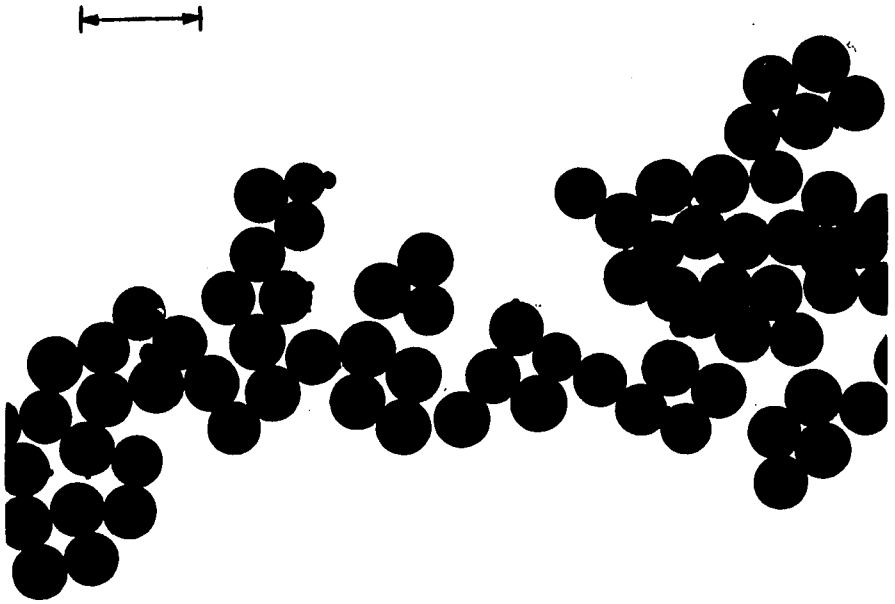

Figure 21. TEM of particles obtained by reacting 450 cm^3 of solution 0.02 M in $Y(NO_3)_3$ and 0.25 M in urea for 1 hr. at 100°C. (bar=1μ)

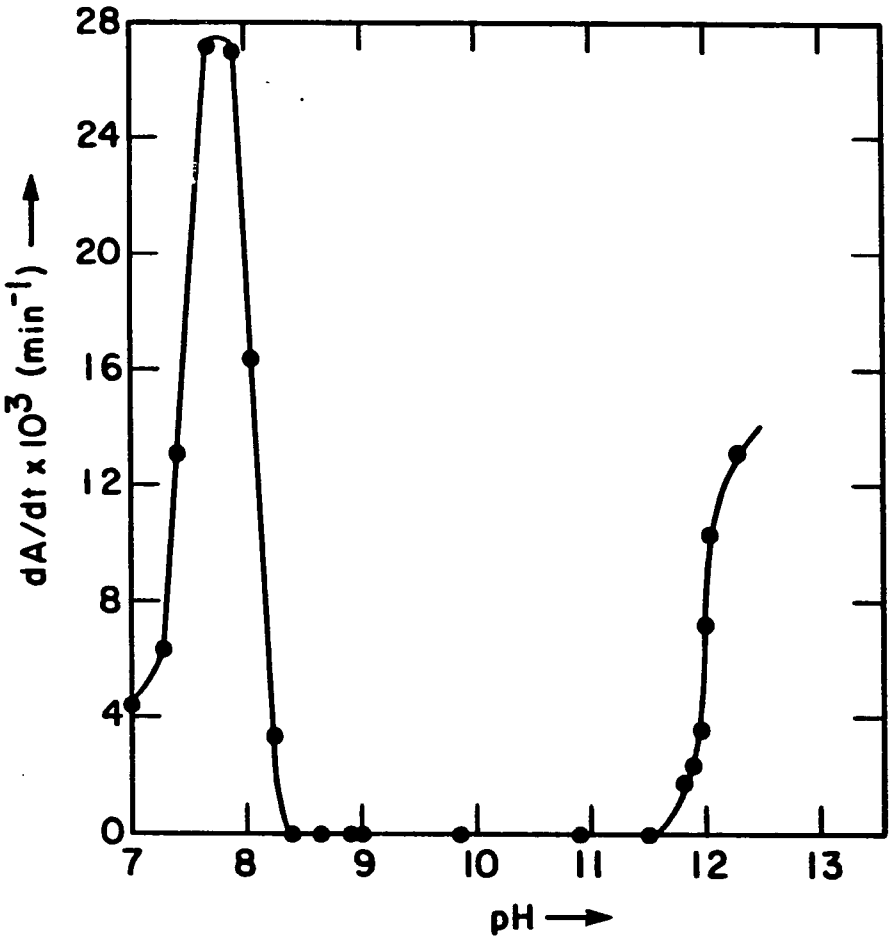

Figure 22. The rate of increase of absorbance (dA/dt) plotted against pH

through 11.6. Beyond a pH of 11.6, flocculation again sets in. This is due to the fact that increasing pH by adding NaOH also increases ionic strength, and above pH 11.6 the ionic strength has increased above 0.004M, appreciably compressing the electrical double layer, shielding particle charges, and thus facilitating sol coagulation.

A satisfactory understanding of the stability of hydrophobic suspensions was reached in the 1940s (74). Using this D.L.V.O theory, the energy of interaction of two spherical particles of radii 0.21μ has been computed as a function of the interparticle center-to-center distance R, for a given pH in the range 7.4 through 12. The purpose in doing this was to establish the experimental conditions that result in the formation of a reasonably deep secondary minimum in an otherwise stable sol. In the absence of exact functions, at the present time, for the repulsive energy V_R, between two spherical particles of radius a, in a medium of dielectric constant ε, the following best approximate equations for small values of the surface potential ψ_o, have been used:

$$V_R = \frac{\varepsilon a \psi_o^2}{2} \ln \{1+\exp(-\kappa(R-2a))\} \qquad [47]$$

in cases where the extension of the double layer is small compared to the radius of the particle, that is $\kappa a >> 1$, where κ is the Debye reciprocal length, given by:

$$\kappa = \left(\frac{8\pi e^2 N_A C z^2}{\varepsilon k T} \right)^{1/2} \qquad [48]$$

where e is the electronic charge, N_A the Avogadro number, C is the electrolyte concentration, z the electrolyte charge number, k the Boltzmann constant, and T the absolute temperature,

$$\text{or} \qquad V_R = \frac{\varepsilon a^2 \psi_o^2}{R} \exp\{-\kappa(R-2a)\} \qquad [49]$$

for cases where $\kappa a << 1$. The expression:

$$V_A = -\frac{A}{6}\left(\frac{2a^2}{R^2-4a^2} + \frac{2a^2}{R^2} + \frac{R^2-4a^2}{R^2} \right) \qquad [50]$$

where A is the Hamaker constant, was used for the energy of attraction, V_A between the particles.

The electrolyte concentrations have been calculated from the pH values, considering NaOH to be the only electrolyte in the suspension. The equations as given above do not take into account the finite size of the ions and the potential to be used in place of the surface potential in calculating the repulsion is the Stern potential. For all practical purposes, ζ-potentials from Figure 5 have been used in lieu of the Stern potentials. In most cases, this approximation, which presupposes that the Stern plane and the slipping plane are (nearly) identical, is good enough. A Hamaker constant value of 10^{-12} ergs has been used. The energy of the barrier (V_{max}) between the particles, the energy of the

secondary minimum (V_{min}), and their positions from the origin (R_{max} and R_{min} respectively) have been plotted as functions of pH in Figures 23 and 24.

Since stability was achieved in the pH range 8.4 through 11.6, it appears that an energy barrier of at least 10^{-12} ergs (24.3 kT) (indicated by a broken line in Figure 23) is required to effectively prevent coagulation. A barrier of about 10 kT is normally considered sufficient to stabilize dispersions against coagulation. Maximum stability is achieved at a pH of 10.8, corresponding to an energy barrier of 68.7 kT and a secondary minimum -1.25 kT deep. From a pH of 7.4 to 10.8, increasing ionization of the surface groups accounts for the increase in V_{max}, while increasing ionic strength is responsible for the decrease in V_{max} beyond 10.8.

In spite of the fact that the cause of particle ordering has been the subject of much debate, we believe that both the secondary minimum and electric repulsion are capable of causing particle ordering. In the presence of a secondary minimum, flocculation in this minimum should result in order formation. This should be possible because the secondary minimum is shallow and not too close to the origin of the interaction energy-distance curve, having the following consequences:

(i) flocculation is not too rapid

(ii) particles in it can dissociate from it quite easily

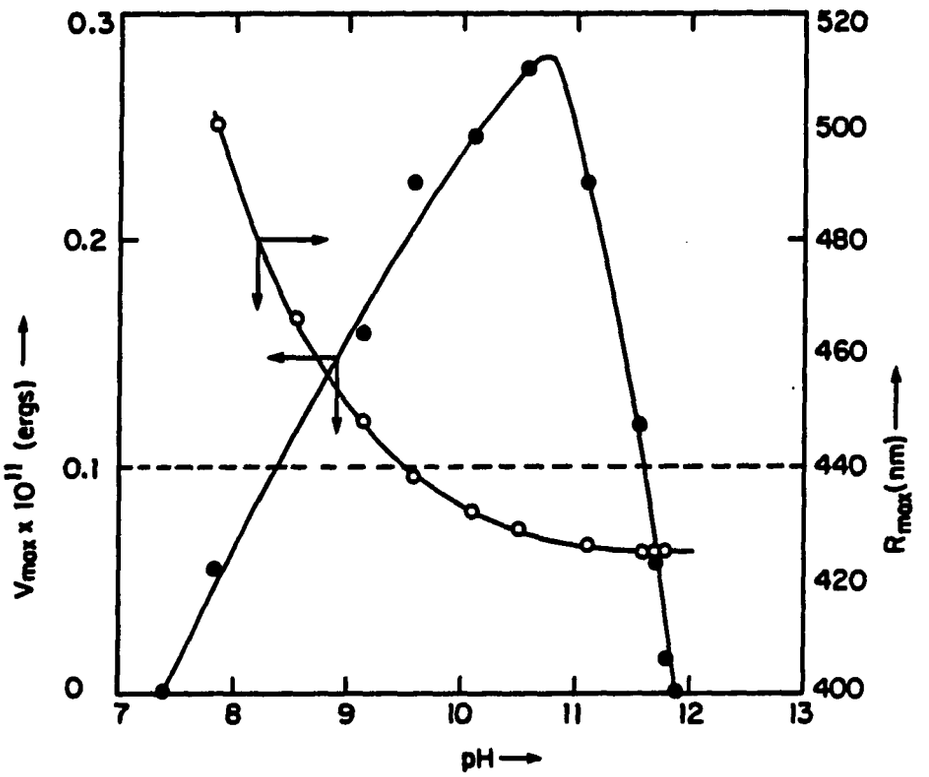

Figure 23. The energy (V_{max}) and position (R_{max}) of the barrier between the particles plotted against pH. Particle radius=0.21μ; Hamaker constant=10^{-12} ergs

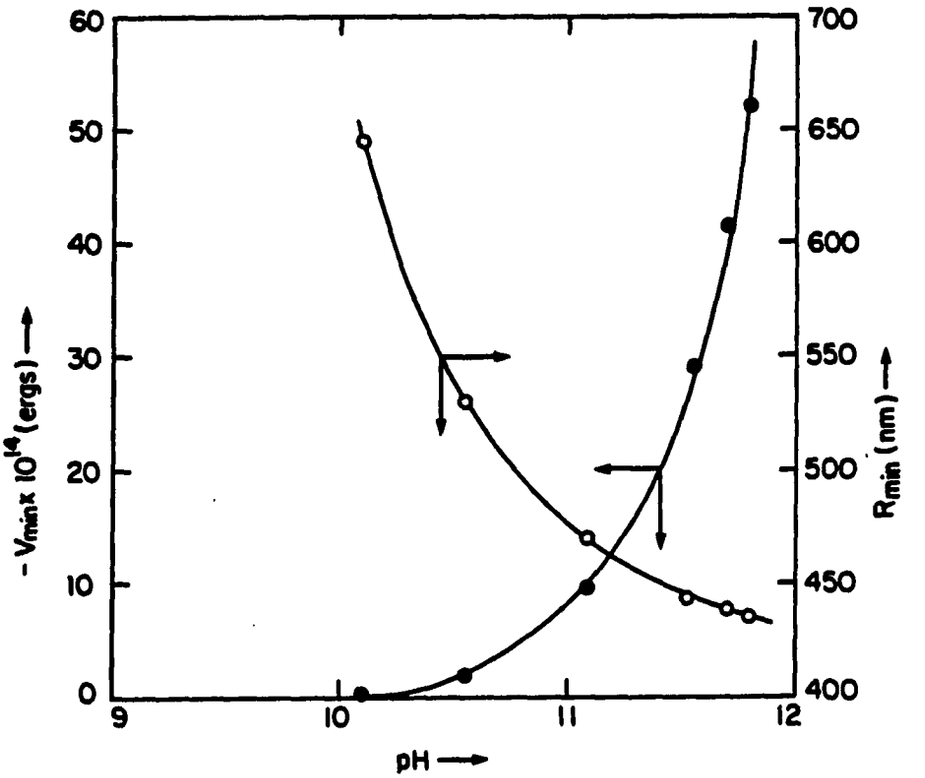

Figure 24. The energy (V_{min}) and position (R_{min}) of the D.L.V.O secondary minimum plotted against pH. Particle radius=0.21μ; Hamaker constant=10^{-12} ergs

kinetically

(iii) particles in it are rather loosely bound, and can easily rearrange and reorganize themselves to produce a highly ordered lattice of minimum free energy and high coordination number

However, ordering produced via this route should result in phase separation. On the other hand, if the forces between the particles are totally repulsive, then particle ordering of the Kirkwood-Alder character (45, 46) should result. According to Kirkwood, in purely repulsive systems, there exists a critical particle concentration above which only crystalline structures with long-range order are possible. Such ordered structures should, therefore, be space-filling.

Ordered structures that are space-filling could also form in the presence of a secondary minimum if the dispersion is so concentrated that the average interparticle distance is smaller than or equal to the separation of the secondary minimum from the origin. Such a system would have to expand if it is to flocculate in the secondary minimum. This is, however, impossible since the system is bound by the volume of the suspension. This situation is illustrated diagramatically in Figure 25.

It, therefore, follows that phase separation (or co-existence of the ordered and disordered phases) is indicative of flocculation in the secondary minimum. On the

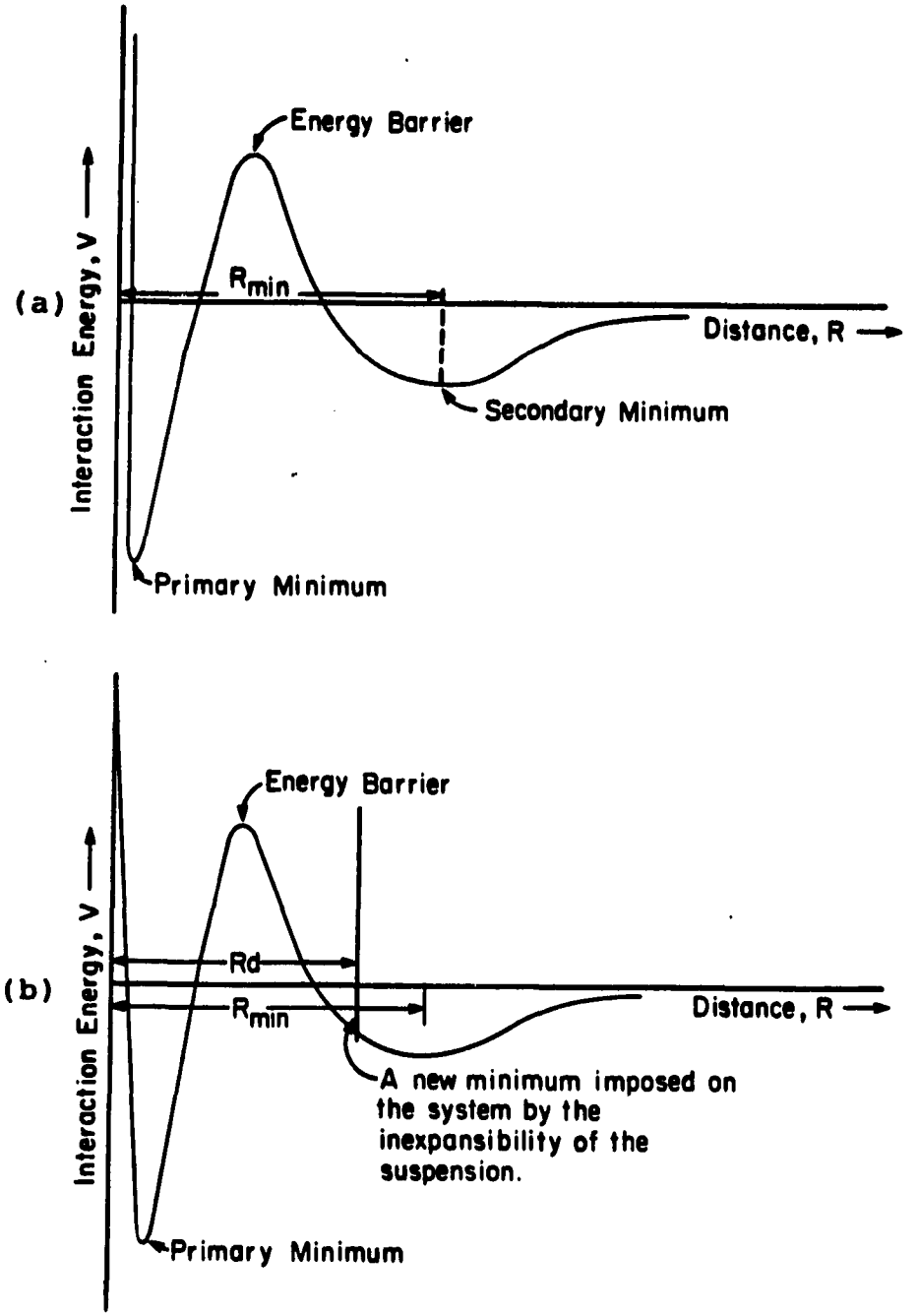

Figure 25. Potential energy-distance curves for (a) a dilute suspension where the position of the secondary minimum (R_{min}) is smaller than the interparticle distance (R_d) (b) a concentrated suspension where the interparticle distance (R_d) is smaller than the position of the secondary minimum (R_{min})

other hand, ordered structures that are space-filling do not only form in totally repulsive systems, but also in the presence of a secondary minimum if a constraint is put on the system such that the interparticle distance is less than or equal to the distance spanned by the secondary minimum.

All the four dispersions left to stand (D1 - D4) had separated into two well defined phases within a week. The upper phase was clear while the lower phase was brightly iridescent. The secondary minimum is, therefore, believed to be responsible for the phase separation with the accompanying order in the lower phase as portrayed by iridescence. This, however, conflicts with the results of the D.L.V.O theory which does not predict the presence of a secondary minimum in D1, D2, and D3 according to Figure 24. This raises serious questions as to the applicability of the D.L.V.O theory to this system. Since the D.L.V.O theory cannot account for our observations, we think like Ise et al. (47, 48), that it may need to be modified to include a coulombic attractive term between the particles, through the intermediary of the counter-ions.

By decreasing the pH of D4 to about 7.4, the energy barrier was supposedly removed, forcing the ordered structure to coagulate rapidly ("freeze") into the primary minimum and the particles to touch. Apparently the order was not destroyed since iridescence (though dull) persisted. Centrifugation afforded maximum particle compaction. Figure

26 shows scanning electron micrographs of the fracture surface of the dried cake. Sputter coating the green cake with a gold film and its subsequent bombardment by the highly energetic electron beam inevitably resulted in cracking. Nevertheless, a high degree of order of particles arranged in a close-packed structure is clearly expressed in the micrographs by the presence of (100) and (111) crystal planes.

The sediment from D5 exhibited dull iridescence suggesting order formation. This was confirmed by microscopic examination of the dry cake, which revealed appreciable close packing of particles (Figure 27). There is, however, some mis-alignment of the particles rendering it difficult to make out the crystal structure of the lattice. The origin of order formation in this system is different though. Despite the presence of the secondary minimum, when the suspension is subjected to a centrifugal force, the particles are forced to approach each other even much closer than the secondary minimum dictates. The centrifugal force, therefore, has a continuous concentrating effect on the suspension. At some stage, the interaction between the particles becomes repulsive and so large that it becomes more energetically favorable to accommodate the particles in an ordered lattice, typical of ordering of the Kirkwood-Alder character.

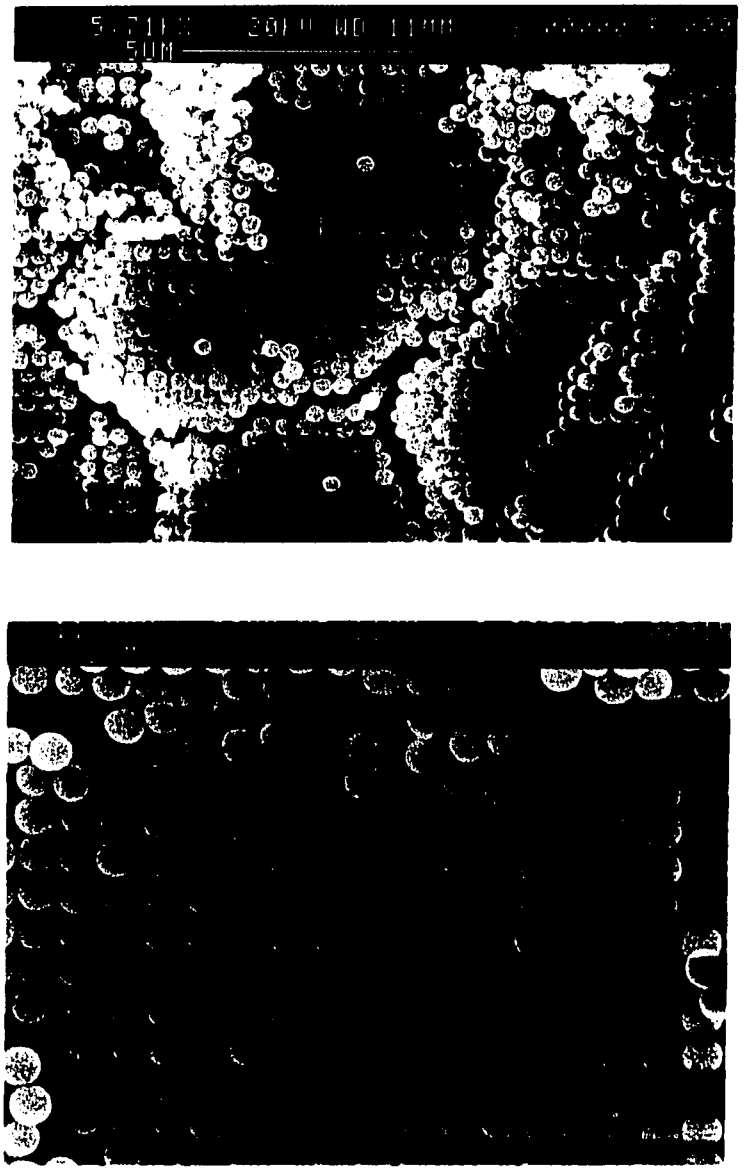

Figure 26. SEMs (at different magnifications) of a fracture surface of a dry cake from the lower iridescent phase (the secondary minimum floc) of suspension D4 (pH 10.9) that separated into two phases upon standing. The floc was coagulated ("frozen") into the primary minimum and further compacted by centrifugation before it was allowed to dry

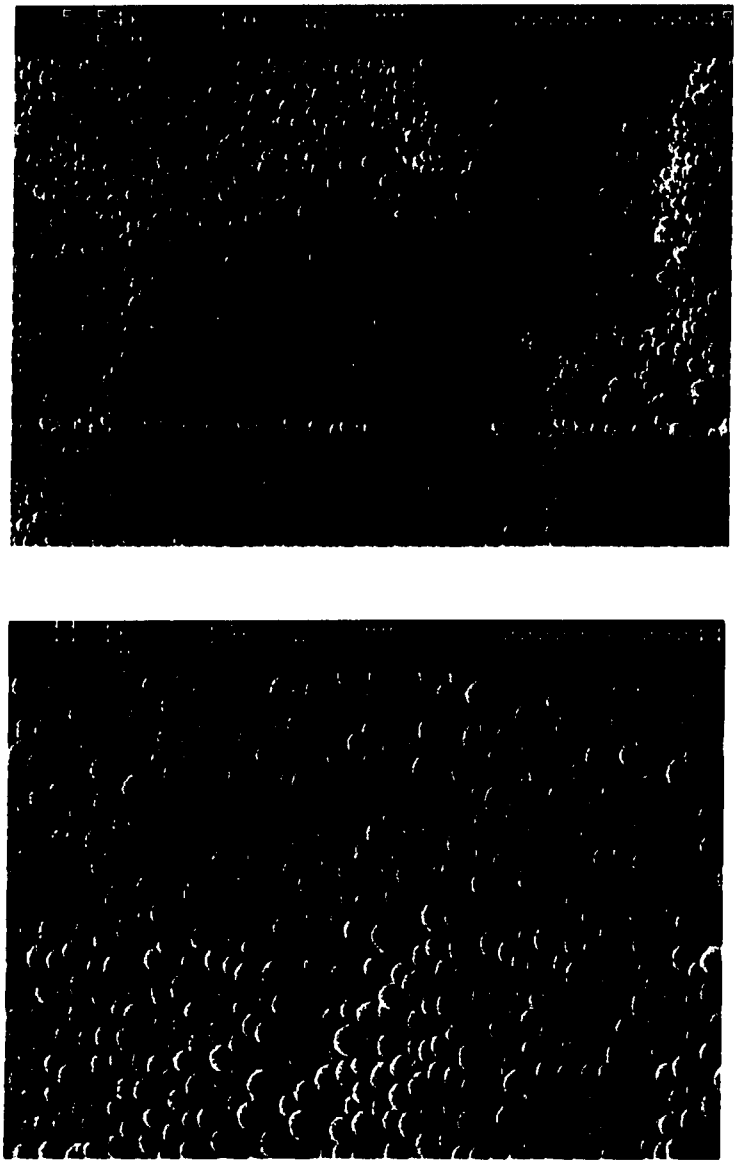

Figure 27. SEMs (at different magnifications) of a fracture surface of a dried iridescent sediment from suspension D5 (pH 10.9) that was spun in a centrifuge at 3000 rpm for 30 min

V. CONCLUSION

The decomposition of urea in aqueous solution of yttrium nitrate at elevated temperatures has been exploited to synthesize spherical colloidal particles of yttrium hydroxy-carbonate of narrow size distribution. It is believed that these particles are formed by a careful control of the homogeneous nucleation and growth processes. Particle sizes and widths of size distributions are functions of reactant concentrations and length of reaction. The particles were found to be crystalline, of composition $Y(OH)CO_3.H_2O$ and density 2.17 g/cm^3. Discrete particles could only be obtained under conditions of low to moderate ionic strengths and if precipitation was not allowed to proceed beyond the coagulation event. Coagulation of the precipitates during preparation is believed to be due to charge neutralization at the particle surface and /or compression of the double layers at high electrolyte concentrations. Particles are otherwise stable with respect to sedimentation. It appears that solution acidity is neutralized before nucleation takes place. For homogeneous precipitation of monosized particles, this system undergoes a single nucleation event which produces about $3X10^{10}$ nuclei/cm^3, followed by diffusion-controlled growth of the particles. In seeded precipitation, pure heterogeneous precipitation takes place if the system contains more than $4X10^{10}$ seeds/cm^3.

Otherwise, in systems containing fewer seeds, homogeneous nucleation proceeds creating enough nuclei to bring the total number to about $4X10^{10}/cm^3$. Aqueous suspensions of these uniform particles are stable within a reasonable range of pH (8.4-11.6). Working within this range, ordered lattices of these particles could be prepared from suspensions with particle volume fraction of 0.2. Particle ordering was attributed to flocculation in the secondary minimum in some suspensions, and to ordering of a Kirkwood-Alder nature in others. A close-packed arrangement of particles ordered in the secondary minimum was observed. For the lattice ordered in the secondary minimum, the IEP was exploited to rapidly "freeze" the structure into the primary minimum, thus forcing the particles to touch. Further compaction of particles was achieved by centrifugation.

VI. REFERENCES

1. Report of the panel on High Temperature Ceramics, U.S. Department of Energy, Materials Science Program, January, 1974.

2. The term "yttrium (hydrous) oxide" is taken here in a rather general sense to include oxides, hydroxides, hydrated oxides, oxyhydroxides, and hydroxy-compounds of yttrium.

3. Darragh, P. J., Gaskin, A. J., and Sanders, J. V., Scient. Am. 234 [4], 84 (1976).

4. Iler, R. K., The Chemistry of Silica (John Wiley, New York, 1979).

5. Matijevic, E., Langmuir 2, 12 (1986).

6. Barringer, E. A., and Bowen, H. K., J. Am. Ceram. Soc. 65 [12], C-199 (1982).

7. Barringer, E. A., and Bowen, H. K., Langmuir 1, 414 (1985).

8. Stober, W., Fink, A., and Bohn, E., J. Colloid Interface Sci. 26, 62 (1968).

9. Tormey, E. S., Pober, R. L., Bowen, H. K., and Calvert, P. D., Advances in Ceramics, edited by Mangers, J. A. et al. (American Ceramic Society Press, Columbus, Ohio, 1984), Vol. 9, p. 140.

10. Ferguson, D. E., Dean, O. C., and Douglas, D. A., The Sol Gel Process for the Preparation and Remote Fabrication of Recycle Fuels. Third U.N int. conf. on the peaceful uses of atomic energy, 11, A/CONF/27/P/237 (1964).

11. Hermans, M. E. A., and Slooten, H. G., The Preparation of UO_2 and ThO_2 Powders in the sub-sieve range. Third U.N int. conf. on the peaceful uses of atomic energy, 11, A/CONF/28/P/634 (1964).

12. Cogliati, G. et al., The Preparation of Dense Particles of Thorium and Uranium Oxide. Third U.N int. conf. on the peaceful uses of atomic energy, 11, A/CONF/28/P/555 (1964).

13. Sol-gel Process for Ceramic Nuclear Fuels, Proceedings of a panel, Vienna, May 1968. (International Atomic Energy Agency, Vienna, 1968).

14. Fletcher, J. M., and Hardy, C. J., Applications of Sol-gel Processes to Industrial Oxides, Chem. Ind. 48 (1968).

15. Woodhead, J. L., Silic. Ind. 37, 191 (1972).

16. Nelson, R. L. et al., Thin Solid Films 81, 329 (1981).

17. Scott, K. T., and Woodhead, J. L., Thin Solid Films 95, 219 (1982).

18. Woodhead, J. L., Sci. Ceram. 10, 169 (1979).

19. Woodhead, J. L., British Patent 1342893 (1974).

20. Woodhead, J. L., British Patent 1181794 (1970).

21. Woodhead, J. L., British Patent 1412937 (1975).

22. Dislich, H., J. Non-Crystalline Solids 73, 599 (1985).

23. Mackenzie, J. D., J. Non-Crystalline Solids 73, 631 (1985).

24. Sakka, S., J. Non-Crystalline Solids 73, 651 (1985).

25. Wenzel, J., J. Non-Crystalline Solids 73, 693 (1985).

26. Scherer, G. W., J. Am. Ceram. Soc. 60 [5-6], 239 (1977).

27. Shimora, T., Makishima, A., Kotani, K., and Wakakura, M., Proc. Int. Symp. of Factors in Densification and Sintering of Oxide and Non-oxide Ceramics, Japan, (1978).

28. Sacks, M. D, and Tseng, T-Y, J. Am. Cer. Soc. 67 [8], 532 (1984).

29. Ciftciouglu, M., Akinc, M., and Burkhart, L., submitted to J. Am. Ceram. Soc.

30. Alfrey, J., Jr., Bradford, E. B., Vanderhoff, J. W., and Oster, G., J. Opt. Soc. Am. 44, 603 (1954).

31. Luck, W., Klier, M., and Wesslau, H., Naturwissenschaften 50, 485 (1963).

32. Luck, W., Klier, M., and Wesslau, H., Ber. Bunsenges. Phys. Chem. 67, 75, 84 (1963).

33. Krieger, I. M., and O'Neil, F. M., J. Am. Chem. Soc. 90, 3114 (1968).

34. Hiltner, P. A., and Krieger, I. M., J. Phys. Chem. 73, 2386 (1969).

35. Hiltner, P. A., Papir, Y. S., and Krieger, I. M., J. Phys. Chem. 75, 1881 (1971).

36. Krieger, I. M., and Hiltner, P. A., Polymer Colloids, edited by Fitch, R. M. (Plenum, New York, 1971).

37. Williams, R., and Crandall, R. S., Phys. Lett. A48, 225 (1974).

38. White, J. W., Top. Curr. Phys. 3, 197 (1977).

39. Daly, J. G., and Hasting, R., J. Phys. Chem. 85, 294 (1981).

40. Kose, A., Ozaki, M., Takano, K., Kobayashi, Y., and Hachisu, S., J. Colloid Interface Sci. 44, 330 (1973).

41. Vanderhoff, J. W., van den Hul, H. J., Tansk, R. J. M., and Overbeek, J. Th. G., Clean Surfaces: Their Preparation and Characterization for Interfacial Studies, edited by Goldfinger, G. (Marcel Dekker, New York, 1970), p. 15.

42. Hiltner, P. A., and Krieger, I. M., J. Phys. Chem. 74, 2386 (1969).

43. Hachisu, S., Kobayashi, Y., and Kose, A., J. Colloid Interface Sci. 42, 342 (1973).

44. Barnes, J. C., Chan, D. Y. C., Everett, D. H., and Yates, D. E., J. Chem. Soc., Trans. Faraday Soc. II. 74, 136 (1978).

45. Kirkwood, J. G., J. Chem. Phys. 7, 919 (1939).

46. Alder, B. J., Hoover, W. G., and Young, D. A., J. Chem. Phys. 49, 3688 (1968).

47. Ise, N., Okubo, T., Sugimura, N., Ito, K., and Nolte, H. J., J. Chem. Phys. 78 [1], 536 (1983).

48. Ise, N., Okubo, T., Ito, K., and Dosho, S., Langmuir 1, 176 (1985).

49. Sogami, I., Phys. Lett. 96 A, 199 (1983).

50. Feynman, R. P., Leighton, R. B., and Sands, M., The Feyman Lectures on Physics 1st. Ed. (Addison-Wesley, Reading, Massachusetts, 1963), Vol. 1, Chap. 2.

51. Walker, J., and Hambley, F. J., J. Chem. Soc. (London) 67, 746 (1895).

52. Fawsitt, C. E., Z. Physik. Chem. 41, 601 (1902).

53. Burrows, G. J., and Fawsitt, C. E., J. Chem. Soc. (London) 105, 609 (1914).

54. Werner, E. A., J. Chem. Soc. (London) 113, 84 (1918).

55. Werner, E. A., J. Chem. Soc. (London) 117, 1078 (1920).

56. Price, T. W., J. Chem. Soc. (London) 115, 1254 (1919).

57. Warner, R. C., J. Biol. Chem. 142, 709 (1942).

58. Krasilshchikov, A. I., J. Phys. Chem. (USSR) 13, 767 (1939); C. A. 34, 7706 (1940).

59. Krasilshchikov, A. I., J. Phys. Chem. (USSR) 13, 1429 (1939); C. A. 35, 371 (1941).

60. Moelwyn-Hughes, E. A., The Kinetics of Reactions in Solution, 2nd Ed. (Oxford, London, 1947), pp. 34, 71, 94, 98, 166.

61. Shaw, W. H. R., and Bordeaux, J. J., J. Am. Chem. Soc. 77, 4729 (1955).

62. Laidler, K. J., and Hoare, J. P., J. Am. Chem. Soc. 72, 2489 (1950).

63. Laidler, K. J., Chemical Kinetics (McGraw-Hill, New York, 1950), p. 130.

64. Particle Size Analysis edited by Stockman, J. D., and Fochtman, E. G. (Pergamon Press, Oxford, 1977).

65. Visca, M., and Matijevic, E., J. Colloid Interface Sci. 68, 382 (1978).

66. Sugimoto, T., and Matijevic, E., J. Colloid Interface Sci. 74, 227 (1980).

67. Matijevic, E., Acc. Chem. Res. 14, 22 (1981).

68. Wilhelmy, D. M., and Matijevic, E., J. Chem. Soc. Faraday Trans. I. 80, 563 (1984).

69. LaMer, V. K., and Dinegar, R. H., J. Am. Chem. Soc. 72, 4847 (1950).

70. LaMer, V. K., and Dinegar, R. H., J. Am. Chem. Soc. 73, 380 (1951).

71. Jean, J. H., and Ring, T. A., Langmuir 2, 251 (1986).

72. Nielsen, A. E., Kinetics of Precipitation (Pergamon Press, Oxford, 1964), p. 36.

73. Maron, S. H., Pierce, P. E., and Ulevitch, I. N., J. Colloid Sci. 18, 470 (1963).

74. Verwey, E. J. W., and Overbeek, J. Th. G., Theory of the Stability of Lyophobic Colloids (Elsevier, Amsterdam, 1948).

VII. ACKNOWLEDGEMENTS

It is a pleasure for me to acknowledge people who have contributed significantly and in many ways to the success of this study.

I wish to express my deepest thanks to my major professor, Dr. Robert Hansen, for his inspiration, support, and guidance throughout my Ph.D. program. My family is indebted to the Hansens for making Ames a habitable place for us upon our arrival during the stormy winter of 1982.

I would like to register my appreciation to the members of my committee, Drs. D. C. Johnson, B. C. Gerstein, O. Buck, and L. E. Burkhart for their cooperation and interest, not only in my work but also in me as an individual. I am particularly thankful to Dr. Burkhart, with whom we have collaborated over the years, for sensitizing us to the problems facing the ceramic processing industry.

I wish to thank my fellow colleagues both "dry" and "wet", past and present; Rudy Klima, Ron Hendershot, Don Dowd, K. G. Baikerikar, Moustafa Seleet, Paul Kleinwolterink, Tommy Lloyd, and Linda Siemsen for their companionship, help, encouragement, and fun.

I am thankful to Fran Laabs, Ed Gibson and Ray Jouett for showing me how to use the various electron microscopes; Jerry Amenson and Glenn Oren for the use of the thermal and

image analysis techniques; Jim Anderegg for performing the XPS analysis, and Bob Bachman for doing the chemical analysis of the powder material. The folks in the graphics and photographic departments of the Ames Laboratory have also been great.

I am also grateful to our many friends at First Evangelical Free Church and those of the International Christian Fellowship for their constant love and support. Their love and prayers sustained us during our stay in Ames.

Our parents, Mr. and Mrs. Kayima, and Mrs. Ssevume; relatives and friends, who prayed and sent their love and encouragement across the seas while we were in the United States, were a constant and sure support for us.

Thanks are also due to our friends and fellow countrymen here in the United States, who have shared not only in our joys, but also in our trials and tribulations.

I am thankful for Katherine (Nina), a precious gift born to us in Ames. She has been and continues to be a source of great joy to us.

Finally, I wish to thank my wife, Jane, who has supported me not only with her labor, but also with things of far greater value: love, patience, and understanding.

VIII. APPENDIX A: FIRST-ORDER RATE CONSTANTS FOR THE DECOMPOSITION OF UREA AT DIFFERENT EXPERIMENTAL CONDITIONS

Temp. /^{o}C	[urea]/M	Medium	First-order rate constant $kX10^{5}/s^{-1}$	Ionic strength /M	Ref
100	$(5.62\text{-}115.4)X10^{-3}$	H_2O	3.80±0.27	-	61
90	$(58.57\text{-}58.59)X10^{-3}$	$0.10MHNO_3$	1.20±1.18	0.100	61
90	$58.71X10^{-3}$	$0.15MHNO_3$	1.06	0.150	61
100	0.5M	$0.50MHNO_3$	1.02	-	53,56

IX. APPENDIX B: THE CHARACTERIZATION AND THE DETERMINATION OF THE NUMBER OF SILICA PARTICLES/CM^3 OF LUDOX SM

A. Characterization of LUDOX SM Colloidal Silica

Average particle diameter	= 7nm
Particle charge	= negative
Stabilizing counter ion	= Na^+ (stabilized with NaOH)
SiO_2 wt%	= 30
PM (25°C)	= 9.9
Specific gravity (25°C)	= 1.22

B. Determination of Silica Particles/cm^3 of LUDOX SM

Let S_p = specific gravity of sol = 1.22

d_w = density of water = 0.9971 at 25°C

d_{sol} = density of sol = $S_p d_w$

w = weight fraction of SiO_2 in sol = 0.30

V = volume fraction of SiO_2 in sol

Consider 1 cm^3 of sol. Its weight is d_{sol}, of which $(1-w)d_{sol}$ is water, occupying a volume $1-V = (1-w)d_{sol}/d_w$. The volume of the SiO_2 is hence:

$$V = 1-(1-w)d_{sol}/d_w = 0.146 cm^3$$

This consists of N particles each of which has a diameter, $d = 7X10^{-7}$, hence a radius, $r = 3.5X10^{-7}$ cm.

Then $N = V/(4\pi r^3/3) = 8.13X10^{17}$ particles/cm^3